NH_2-truncated human tau induces deregulated mitophagy in neurons by aberrant recruitment of Parkin and UCHL-1: implications in Alzheimer's disease

V. Corsetti[1], F. Florenzano[2], A. Atlante[3], A. Bobba[3], M.T. Ciotti[4], F. Natale[4], F. Della Valle[4], A. Borreca[4], A. Manca[2], G. Meli[2], C. Ferraina[2], M. Feligioni[2], S. D'Aguanno[4], R. Bussani[5], M. Ammassari-Teule[4], V. Nicolin[6], P. Calissano[2,†] and G. Amadoro[1,2,†,*]

[1]Institute of Translational Pharmacology (IFT) – National Research Council (CNR), Via Fosso del Cavaliere 100-00133, Rome, Italy, [2]European Brain Research Institute (EBRI), Via del Fosso di Fiorano 64-65, 00143 Rome, Italy, [3]Institute of Biomembranes and Bioenergetics (IBBE)-CNR, Via Amendola 165/A, 70126 Bari, Italy, [4]Institute of Cellular Biology and Neuroscience (IBCN)-CNR, IRCSS Santa Lucia Foundation Via del Fosso di Fiorano 64-65, 00143 Rome, Italy, [5]UCO Pathological Anatomy and Histopathology Unit, Cattinara Hospital Strada di Fiume 447, 34149 Trieste, Italy and [6]Department of Medical, Surgical and Health Science, University of Trieste, Strada di Fiume 449, 34149 Trieste, Italy

*To whom correspondence should be addressed at: Institute of Translational Pharmacology (IFT) – National Research Council (CNR), Via Fosso del Cavaliere, 100-00133 Rome, Italy. Tel: +39 06501703269; Fax: +39 06501703313; Email: g.amadoro@inmm.cnr.it

Abstract

Disarrangement in functions and quality control of mitochondria at synapses are early events in Alzheimer's disease (AD) pathobiology. We reported that a 20–22 kDa NH_2-tau fragment mapping between 26 and 230 amino acids of the longest human tau isoform (aka NH_2htau): (i) is detectable in cellular and animal AD models, as well in synaptic mitochondria and cerebrospinal fluids (CSF) from human AD subjects; (ii) is neurotoxic in primary hippocampal neurons; (iii) compromises the mitochondrial biology both directly, by inhibiting the ANT-1-dependent ADP/ATP exchange, and indirectly, by impairing their selective autophagic clearance (mitophagy). Here, we show that the extensive Parkin-dependent turnover of mitochondria occurring in NH_2htau-expressing post-mitotic neurons plays a pro-death role and that UCHL-1, the cytosolic Ubiquitin-C-terminal hydrolase L1 which directs the physiological remodeling of synapses by controlling ubiquitin homeostasis, critically contributes to mitochondrial and synaptic failure in this *in vitro* AD model. Pharmacological or genetic suppression of improper mitophagy, either by inhibition of mitochondrial targeting to autophagosomes or by shRNA-mediated silencing of Parkin or UCHL-1 gene expression, restores synaptic and mitochondrial content providing partial but significant protection against the NH_2htau-induced neuronal death. Moreover, in mitochondria from human AD synapses, the endogenous NH_2htau is stably associated with Parkin and with UCHL-1. Taken together, our studies show a causative link between the excessive mitochondrial turnover and the NH_2htau-induced *in vitro* neuronal death, suggesting that pathogenetic tau truncation may contribute to synaptic deterioration in AD by aberrant recruitment of Parkin and UCHL-1 to mitochondria making them more prone to detrimental autophagic clearance.

† These authors equally contributed to this work.

Accepted: February 10, 2015

Introduction

N-terminal truncation of tau is an early event in Alzheimer's disease (AD) and not-AD tauopathies (1–4). Mitochondrial dysfunction (5–9) as well as unbalance in protein ubiquitylation/de-ubiquitylation (10–13) are chronic and precipitating mechanisms underlying the tau-induced synaptic degeneration which has been shown to be closely correlated to impaired cognitive function and memory loss in AD pathology (14,15). Cellular and transgenic AD models have shown that Aβ and tau can in independent and/or synergic way(s) adversely affect metabolism of mitochondria-including alteration in their trafficking, dynamics and clearance (16–23)-favoring bioenergetic failure and synapses loss (24–26). In the last few years a deregulated turnover of mitochondria (27–29), which leads to a reduction in their biomass and metabolic capacities, has been described to take place into vulnerable neurons and synapses from AD brains (30–33) as well as from AD transgenic mice (34), thus supporting strategies aimed at preserving a proper quality control of these organelles as novel and promising disease-modifying interventions in therapy of this devastating disease (35,36). However, the exact and causal role of unbalanced mitophagy in neurodegeneration is still largely debated. In fact, on the one hand, autophagic elimination of mitochondria plays a neuroprotective role under conditions of acute and/or mild stress or at the beginning of insult, when elimination of damaged mitochondria can be properly counterbalanced by an equivalent functional reserve of these organelles through a homeostatic induction of their biogenesis (37,38). On the other hand, under exposure to lethal and/or chronic injuries, the overactivated removal of mitochondria exceeds the normal regenerative capacity of mitochondrial biogenesis and, consequently, massive mitophagy turns out to be neurotoxic leading to an insufficient amount of intact and respiration-competent mitochondria which, eventually, causes 'mitophagic' death particularly in suffering or aged neuronal populations (39–43).

Compelling *in vitro* and *in vivo* evidence has also indicated that the free pool of ubiquitin represents an unifying cellular hub linking the two major intracellular proteolytic systems, the ubiquitin-proteasome system (UPS) and the selective autophagy (44,45), and that a tight control of ubiquitin steady levels is of great importance for synaptic homeostasis and neuronal survival (12). Actually the Parkin-driven mitophagic pathway, a selective form of autophagy which is crucial in maintaining an healthy and energetic-competent mitochondrial network in post-mitotic neurons mainly at ATP-consuming synapses (38,46–48), relies not only on the ubiquitylation of several mitochondrial outer membrane proteins (49–53) but also on direct recruitment and activation of UPS components onto mitochondria (54–57). Among members belonging to family of neuron-specific deubiquitinating enzymes (DUBs), Ubiquitin-C-terminal hydrolase L1 (UCHL-1,PGP9.5) is the most abundant (1–2% of soluble brain proteins) and multifunctional one, being endowed with two different activities: it can act both as hydrolase, by removing and recycling ubiquitin molecules from target proteins, and as ubiquityl ligase, by generating polyubiquitin chains which tag them for disposal. Moreover, UCHL-1 is also able to associate with ubiquitin to inhibit its degradation in neurons (58) and therefore its primary role at synapses (59,60) is to critically control their structure and/or functions by locally maintaining ubiquitin homeostasis *in vitro* as well as *in vivo* (61,62). An impaired activity of UCHL-1 has been proved to be linked to synaptic failure in AD neurodegeneration (63–66) and its immunoreactivity is prominently detected in tau-laden, tangles-bearing neurons which are located in selectively vulnerable and affected regions (65,67,68). Interestingly, the ubiquitin E3 ligase Parkin and other proteins involved in mitochondrial energy metabolism and/or *glycolysis* have been recently identified as UCHL-1 interacting proteins (69,70), suggesting that this enzyme may serve in neurons as a possible modifier in Parkin-dependent mitochondrial turnover. However, whether dysregulation in UCHL-1 activity can actually predispose to AD neurodegeneration by adversely affecting mitochondrial dynamics at synapses is still unknown.

We have previously reported that a NH_2-26-230 tau fragment (s) (aka NH_2htau), mapping between 26 and 230 amino acids of the longest human isoform (htau40): (i) is neurotoxic in primary cultured neurons (71,72); (ii) is detected in cellular and animal AD models (73), as shown by other authors (74–76); (iii) is largely enriched in human mitochondria from AD synaptosomes, in correlation with synaptic disarrangement, with load of Aβ oligomers and with organelle functional impairment (77). The 20–22 kDa NH_2htau, but not the physiological full-length protein, preferentially interacts with Aβ peptide oligomers at human AD synapses and cooperates with them in inhibiting the adenine nucleotide translocator-1 (ANT-1)-dependent ADP/ATP exchange at mitochondria (17). Moreover, the NH_2htau fragment is also present outside neurons in peripheral CSF from living patients affected by tau-dependent neurodegenerative diseases associated with dementia, providing a novel biomarker for AD and not-AD human tauopathies (78). Interestingly, *in vivo* expression of NH_2htau fragment activates a non-apoptotic cell death pathway causing in transgenic mice severe defects of hippocampal neurogenesis in connection with an increased anxiety-behavior and impaired episodic-like memory (79). Finally, an extensive Parkin-dependent autophagic clearance of mitochondria (mitophagy) occurs in NH_2htau, expressing post-mitotic neurons in concomitance to bioenergetic deficits and synaptic damages (80).

In order to better clarify the molecular mechanisms underlying the NH_2htau-induced perturbations in quality control of neuronal mitochondria and to understand how this deregulated mitophagy could be related to AD neurodegeneration, here we show, by cell-based and *in vivo* approaches, that: (i) the Parkin-dependent mitophagy plays a pro-death role in NH_2htau-expressing post-mitotic neurons and (ii) UCHL-1 is a critical mediator of mitochondrial decline and synaptic failure.

Results

Pharmacological and genetic inhibition of mitochondrial quality control preserves the loss of mitochondrial proteins, significantly attenuating the NH_2htau-induced *in vitro* neuronal death

We reported that NH_2htau early affects the quality control of mitochondria in post-mitotic neurons leading to: (i) net reduction in their mass in correlation with a general Parkin-mediated remodeling of membrane proteome; (ii) their extensive association with LC3 and LAMP1 autophagic markers; (iii) bioenergetic deficits and (iv) *in vitro* synaptic pathology (80). However, whether the NH_2htau-enhanced autophagic turnover of mitochondria exacerbates neuronal death because of depletion of functional mitochondria or, alternatively, is a compensatory attempt to mitigate neuronal damage, still remains to be clarified. Therefore, with the intent of evaluating whether the increased mitochondrial clearance occurring in NH_2htau-expressing neurons may be beneficial or rather toxic, we interfered with mitochondria loss in two alternative but complementary ways: (1) by blocking the autophagic machinery directly; (2) by up-regulating the intracellular levels of Mitofusin 2 (Mfn2) and OPtic Atrophy-1 (OPA-1), two proteins

which directly control the mitochondrial dynamics and whose reduction in expression has proved to facilitate the mitophagy (81–83), as detectable in NH_2htau-expressing neurons (80).

Initially, we tested in our *in vitro* neuronal model the potential action on neuronal viability of three different and selective autophagic inhibitors, bafilomycin A1 (BAF-A1), 3-methyladenine (3MA) and cloroquine (CQ), which interfere with degradative autophagic flux of mitochondria by inhibiting the early autophagosomes formation, acidification and late fusion to lysosomes. BAF-A1 is a cell-permeable, selective inhibitor of vacuolar-type (v-type) H+ ATPase while 3MA is another autophagic inhibitor which upstream blocks the autophagosomes sequestration, acting on class III phosphatidylinositol 3-kinases (PI3K). CQ is an alkalizing reagent, such as BAFA1 and NH_4Cl, used to raise the lysosomal pH, which leads to inhibition of both fusion of autophagosome with lysosome and lysosomal protein degradation. The effect on neuronal viability of these drugs, which were used at different concentrations reported in the literature to inhibit mitophagy (84–87), was compared with that of 10 μM FCCP (carbonyl cyanide 4-(trifluoromethoxy)phenylhydrazone), a protonophore (H^+ ionophore) which induces mitochondria fragmentation and their selective removal by mitophagy (52,53). To this aim, mature hippocampal primary neurons (DIV 15) were transduced (75% efficiency) by adenovirus-mediated infection with myc-tagged NH_2-26-230 tau (myc-NH_2htau) or with myc-tagged empty vector (mock) at low/moderate multiplicity (MOI 50), in presence or in absence of drugs, and, at 16 h post-infection, viability was assessed by MTT assay, a detection system that is widely accepted as valuable readout for mitochondrial energy production (88). In agreement with our previous investigations (72,80), the specific expression of exogenous myc-NH_2htau in cultured neurons negatively impinged on their survival thus only 60% of cells was still alive under these *in vitro* experimental conditions. On the contrary, no significant difference in viability was found upon transduction with mock or unrelated LacZ-protein (not shown). As assessed by MTT assay (Fig. 1A) and intact nuclei count (not shown) and in line with other *in vitro* and *in vivo* neuronal models associated with deregulated mitophagy (39,41,42,86), pharmacological suppression of autophagic pathway with BAF1 and CQ and less with 3MA provided partial but significant protection at 16 h post-infection, by improving viability of NH_2htau-expressing cultures (MOI 50) but not of control ones (MOI 100). On the contrary, FCCP drastically sensitized NH_2-htau-infected cultures by further aggravating neuronal death. No rescuing-action was afforded by treatment of our *in vitro* neuronal model cultures with 10 μM rapamycin, an antibiotic reported to stimulate autophagy via inactivation of mammalian Target Of Rapamycin (mTOR) serine/threonine protein kinase (not shown). Relevantly, the protection against the NH_2htau-induced death offered by treatment with 3-MA is smaller than that provided by BAF-A1 and CQ, indicating that the induction of autophagy in our neuronal cultures is initiated at mitochondria themselves with only a minor contribution of general up-regulation of macroautophagy.

It has been proposed that: (i) inhibition of Mfn2-stimulated fusion of mitochondria contributes to enhance the rate and/or selectivity in quality control of these organelles during Parkin-driven mitophagy (89); (ii) transduction with Mfn2 prevents mitochondrial fragmentation thereby maintaining neuronal survival after injury (83,90); (iii) loss of normal Mfn2 function leads to autophagic removal of mitochondrial mass in cultured primary neurons (82). As the intracellular levels of Mfn2 are found to decline in NH_2htau-expressing neurons in concomitant with pronounced cell death and with deregulated autophagic flux of small and fragmented mitochondria (80), we next tested whether up-regulation of this mitochondrial-reshaping protein was able to promote neuronal survival, by compensating/balancing for reduction in length of mitochondria and, then, by counteracting their loss in mass (91). As shown in Figure 1B and in line with the protective role of Mfn2 in preventing mitochondrial fragmentation and consequential cell death in several *in vitro* models of neuronal injury (90), viability in NH_2htau-expressing neurons was significantly relieved at 16 h post-infection (MOI50) if these cultures were formerly transfected (24 h before) with wild-type Mfn2-coding plasmid (FlagwtMfn2) but not with mock one (Flag peptide tag), used as internal control. Western blotting analysis and immunofluorescence experiments with anti-Flag (M2) and anti-Mfn2 antibodies, respectively, were done to check the successful efficiency of exogenous transgene delivery in our tau-transduced neuronal cultures and the up-regulation of intracellular levels of total Mfn2 (Supplementary Material, Fig. S1).

Mitochondria play a central role in directing cell death signaling generated by excessive activation of NMDAR (*N*-methyl-D-aspartate receptor) occurring during cerebral ischemia, seizures, chronic AD neurodegeneration and sustained stimulation of extrasynaptic, NR2B-enriched NMDAR takes place in NH_2htau-expressing neurons, leading to a fatal calpain-I activation which in turn critically controls viability during excitotoxic injury (72). Excessive activation of calpain-I early occurs in AD neurodegeneration in response to calcium injury underlying Aβ-mediated synaptic decay (92), likely due to marked depletion of its specific endogenous inhibitor calpastatin (CAST) (93). Furthermore, several studies indicate that OPA-1 knockdown provokes the autophagic removal of mitochondria without interfering with their transport (82) and that calpastatin promotes neuronal survival against excitotoxicity (94) by blocking mitochondrial fragmentation upstream of OPA-1 function(s). As cell death occurring in NH_2htau-expressing neurons is paralleled by a significant reduction in intracellular levels of OPA-1 in association with a severe enlargement of inner membrane cristae of mitochondria (80), we further tested whether the calpain-mediated loss of OPA-1 function could also be causally related to alterations in mitochondrial dynamics and in survival in our *in vitro* AD model. To validate our hypothesis, we attempted to compensate for the intracellular decline of OPA-1 turning to Tg-hCAST mice, transgenic mutants (Tg) which overexpress human calpastatin (hCAST) under control of a calcium–calmodulin-dependent kinase II α promoter. Importantly, genetic modulation of calpastatin expression levels in Tg-hCAST transgenic model did not cause any significant defect in development, fertility, morphology or life-span of these mice under normal conditions, indicating that calpastatin is mainly a negative regulator of calpain but only under pathological conditions (95,96). We expressed the NH_2htau fragment (MOI 50) in hippocampal primary neurons obtained from heterozygous Tg-hCAST mice (Tg/+) (Fig. 1C and D) to investigate whether the rescue of endogenous OPA-1 levels, due to calpastatin-mediated *in vivo* inhibition of calpain (94), could improve their viability. As shown in Figure 1E and F by MTT assay and intact nuclei count, a virtually complete neuroprotection from the NH_2htau-induced death was observed at 16 h post-infection in Tg/+ hippocampal cultures when compared with wild-type littermate (+/+) ones. Note that, consistently with their improved survival, content of mitochondrial marker OPA-1 (Fig. 1G and H) was significantly preserved in NH_2htau-expressing neurons from Tg/+ mice compared with +/+ ones suggesting that defects in mitochondrial dynamics are precipitating, causative events underlying excitotoxic signaling occurring in these *in vitro* experimental conditions. Nevertheless, the extent of

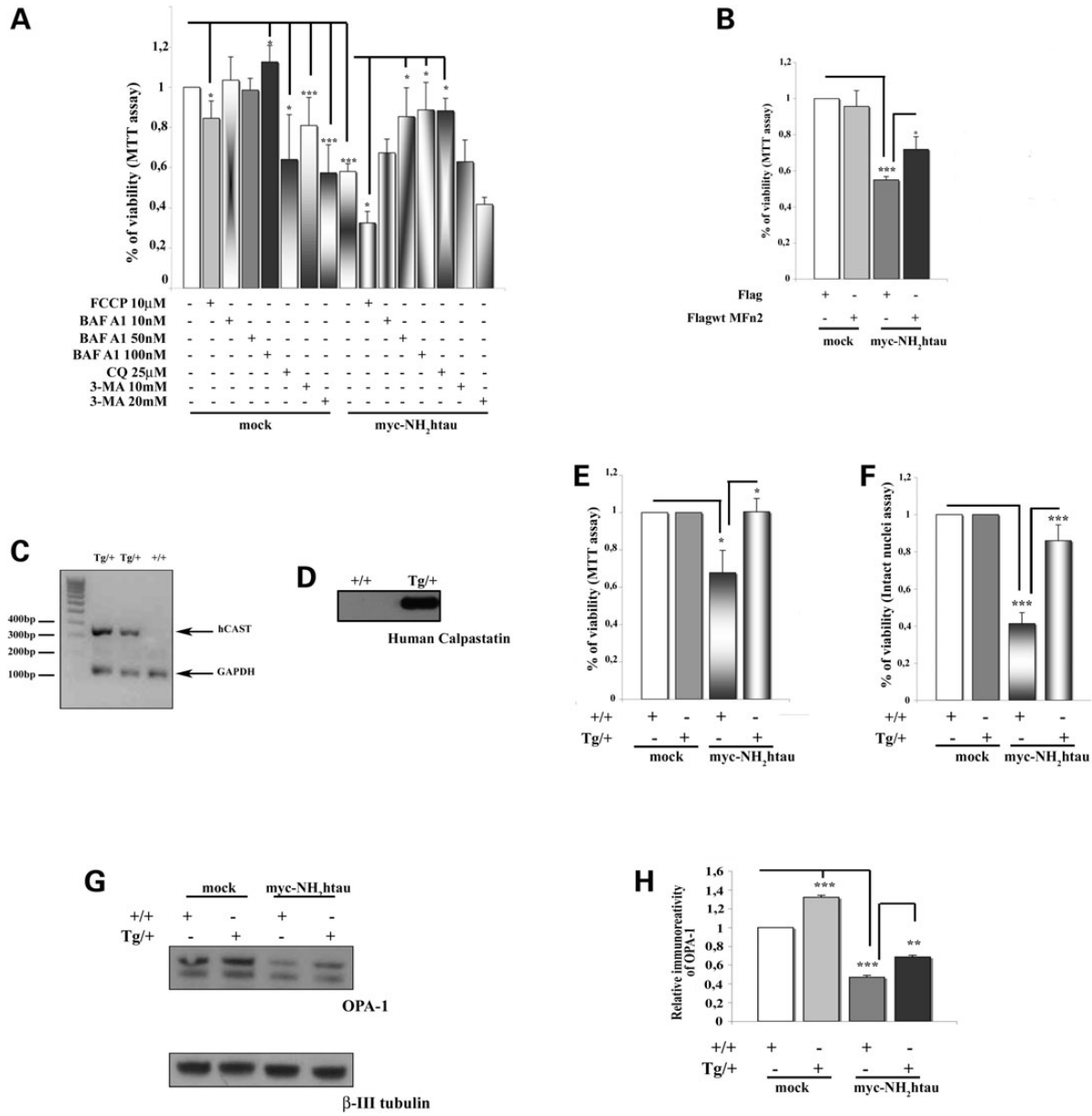

Figure 1. Genetic modulation of mitochondrial dynamics provides moderate but significant neuroprotection from NH_2htau-induced death. (**A**) Graph shows neuronal viability, evaluated by mitochondria-based MTT assay on hippocampal primary neurons (DIV 15) adenovirally transduced with myc-NH_2htau (MOI 50) or with mock control (MOI 100) and examined at 16 h post-infection, in absence or in presence of different autophagic inhibitors used at the indicated concentrations. Values are means of nine independent experiments and statistically significant differences were calculated by unpaired two-tailed Student's *t*-test (*$P < 0.05$; ***$P < 0.0001$). (**B**) Hippocampal primary neurons were transfected by Nucleofector kit (AMAXA) for 24 h with plasmid expressing Flag-tag alone, as internal control, or Flag-tagged wtMfn2 and then infected with myc-NH_2htau (MOI 50) and with mock control (MOI 100) for additional 16 h. Neuronal viability was evaluated by MTT assay. Values are means of three independent experiments and statistically significant differences were calculated by unpaired two-tailed Student's *t*-test (*$P < 0.05$; ***$P < 0.0001$). (**C** and **D**) Representative genotype test by PCR analysis (C) showing the specific 350 bp band of hCAST in heterozygous transgenic mice (Tg) that overexpress the human calpastatin (hCAST) construct (Tg/+). Only the 100 bp band of GADPH internal control was present in WT littermates (+/+). Immunoblot analysis using an antibody specific for hCAST (200) confirms the expression of human calpastatin protein in cultures from Tg/+ transgenic animals, with no detectable levels in +/+ littermates (D). (**E** and **F**) Primary hippocampal neurons (DIV 15), obtained from heterozygous transgenic mice (Tg) that overexpress the human calpastatin (hCAST) construct (Tg/+) or from WT littermates (+/+), were infected with myc-NH_2htau (MOI 50) and with mock control (MOI 100) for 16 h. Neuronal viability was evaluated by MTT assay (E) and intact nuclei count (F). Values are means of three independent experiments and statistically significant differences were calculated by unpaired two-tailed Student's *t*-test (*$P < 0.05$; ***$P < 0.0001$). (**G** and **H**) Representative blot of western blotting analysis ($n = 3$) on total protein extracts from hippocampal primary neurons (DIV 15) that overexpress the human calpastatin (hCAST) construct (Tg/+) or from WT littermates (+/+), infected at MOI 50 for 16 h with myc-NH2htau (MOI 50) and with mock control (MOI 100) to assess the content of the mitochondria marker OPA-1. β-III tubulin was used as loading control (G) and densitometric quantification was performed (H). Values are means of three independent experiments and statistically significant differences were calculated by unpaired two-tailed Student's *t*-test (*$P < 0.05$; ***$P < 0.0001$ versus mock; **$P < 0.01$ versus NH2htau/+/+).

protection afforded by the calpastatin overexpression in neurons was much greater than that observed by wtMfn2 overexpression implicating that, as we and others previously reported (72,97), other mechanisms acting on direct calpain-inhibition can promote survival of injured NH_2htau-expressing cultures. Alternatively, neuroprotection provided by wtMfn2 overexpression

was significant but not complete owing to residual toxicity of mitochondria-targeted NH_2htau on ANT-1-mediated ADP/ATP exchange.

Altogether these data demonstrate that pharmacological and genetic suppression of mitophagy provides partial but significant protection against the NH_2htau-induced neuronal death, pointing out that neuronal demise induced *in vitro* by the enhanced intracellular levels of NH_2htau, as we detected *in vivo* in human AD brains (18,77), is at least in part due to an excessive induction of signaling pathway(s) for quality control of mitochondria.

Parkin plays a critical role in mitophagy in NH_2htau-dying neurons

Recruitment of the endogenous Parkin onto depolarized mitochondria—which is early detected in our NH_2htau expressing cultured neurons undergoing increased mitophagy, synaptic changes and cell death (80)—is critically required in mature neurons for selective elimination of mitochondria through the autophagy-lysosomal pathway (50,52,53,57,98,99). Furthermore, hexokinase activity triggers mitophagy in post-mitotic neurons as it upstream controls relocalization of Parkin to defective mitochondria and supports glycolysis, allowing for ATP synthesis (98,100). For these reasons, we first tested whether the moderate (MOI 50) and early *in vitro* expression of NH_2htau fragment positively elevated hexokinase activity in our 16 h-infected primary neurons. As shown in Figure 2A, which reports values assessed in total cell homogenates (for detail see methods) from mock- and NH_2htau-tranduced group, a significant increase in hexokinase activity (normalized to total homogenate proteins content) was detected in NH_2htau-infected cultures when compared with controls, consistently with finding that a robust Parkin-mediated mitophagy in neurons is strictly dependent on their bioenergetic status (98,100). Importantly, variations in hexokinase activity took place in NH_2htau-expressing neurons regardless of equivalent abundance of protein, as checked by western blotting analysis on whole-cell extracts (Fig. 2A), proving thus that its up-regulation under our *in vitro* conditions was not attributable to differences in intracellular expression levels but rather to a truly positive modulation in enzymatic activity.

In view of the fact that our pharmacological and genetic data demonstrated that deregulated mitophagic pathway was causally involved in our *in vitro* AD model (Fig. 1), we next analyzed whether Parkin was actually associated with NH_2htau-induced cell death by accelerating lysosomal-mediated clearance of mitochondria. To address this possibility, mitochondrial dyshomeostasis as well as loss in synaptic content and cell viability were monitored in our tau-transduced cultures after specific target-gene silencing with small hairpin (sh)RNA plasmid for Parkin expression. Consistently with the protective role of Parkin suppression in another cellular paradigm of neurodegeneration characterized by excessive mitophagy following the *in vitro* overexpression of mutant A53T α-synuclein (41), we found that neuronal survival evaluated at 16 post-infection by MTT assay was significantly improved in NH_2htau-expressing neurons (MOI 50) by shRNA knock-downing of Parkin (48 h before). On the contrary, no rescue in viability was afforded by non-target shRNA (shRNA scrambled), used as negative internal control (Fig. 2B). High-efficiency of Parkin silencing was checked by western blotting analysis followed by densitometric quantification (Fig. 2C and D) and no change in protein levels of myc-NH_2htau was detected after shRNA treatment of neuronal cultures up to 48 h (Fig. 2E). More importantly, specific inhibition of Parkin expression, which is *per se* relatively nontoxic in primary neurons (41), not only partially reverted cell death in NH_2htau-infected cultures but also suppressed the drop in mitochondrial as well in synaptic protein content, as shown by western blotting with OPA-1 and synapsin I antibodies respectively (Fig. 2E).

We have previously reported that neither clearance of defective mitochondria and, consequently, nor significant cell death are detected upon NH_2htau overexpression in HeLa (80), a cell line which has little or no endogenous expression of Parkin (87,101,102). In order to definitively validate the pro-death role of Parkin under these experimental *in vitro* conditions, we tested whether ectopic expression of a specific Parkin-coding plasmid in HeLa cell type could restore susceptibility to NH_2htau-induced mitochondrial injury. As shown in Figure 2F, viability assessed by MTT assay was significantly affected at 16 h post-infection (MOI 50) if HeLa cells were exogenously endowed (24 h before) with expression vector for Parkin protein. Confocal microscopy (Fig. 2G) was carried out to check the efficiency (~75%) of successful delivery of exogenous mCherry Parkin transgene in this cell line.

Altogether these findings indicate the hexokinase-dependent, Parkin-overdriven mitophagy crucially affects synapses stability and, then, cell viability in *in vitro* NH_2htau-expressing neurons.

UCHL1 relocalizes to mitochondria and critically contributes to their deregulated autophagic elimination in NH_2htau-expressing neurons

Accumulating evidence reveals that the efficient removal of dysfunctional mitochondria can be achieved by the synergistic and/or parallel actions of UPS and autophagic-lysosomal pathway (54–56) and that the UPS components are directly recruited and activated on mitochondria during Parkin-dependent mitophagy (55). Intriguingly, activation, translocation and enzymatic functions of Parkin during mitochondrial quality control are controlled by ubiquitylation (103–105) and reversible monoubiquitination negatively regulates the activity of UCHL-1 (106). Besides, proteomic approaches have recently identified UCHL-1 as a novel Parkin-binding partner in SH-SY5Y neuronal cell line undergoing FCCP-induced mitophagy (69,70), consistently with its ubiquitin-stabilizing activity in neurons (58).

In view of the above-mentioned considerations, we set out to establish whether UCHL-1 actually served as modifier in the Parkin-dependent mitophagy occurring in NH_2htau-expressing neurons. To this aim, we first investigated whether clearance of mitochondria following the moderate expression of NH_2htau fragment was associated with recruitment of UCHL-1 to mitochondria, in a similar way to that we reported to occur in our *in vitro* model for Parkin which targets these organelles triggering thus their autophagic elimination (80). As shown by biochemical separation of crude cytosolic/mitochondrial proteins obtained from 16 h-infected neurons (Fig. 3A), we found that a stable proportion of UCHL-1 was distributed at mitochondria in our tau-transduced neurons because it was partially recovered in mitochondria-enriched fractions. Notably, the mitochondrial relocalization of UCHL-1 occurred in connection with that of both overexpressed myc-NH_2htau (MOI 50) and endogenous Parkin which, in agreement with our previous investigations (80), appeared nearly excluded from corresponding cytosolic compartments. Consistently with our biochemical results, confocal analysis (Fig. 3B and B′) performed on 16 h-infected hippocampal cultures (MOI 50) following double immunofluorescence with UCHL-1 (green) and Tomm20 or Grp75 (red), which are two different mitochondrial markers used routinely to detect activation of

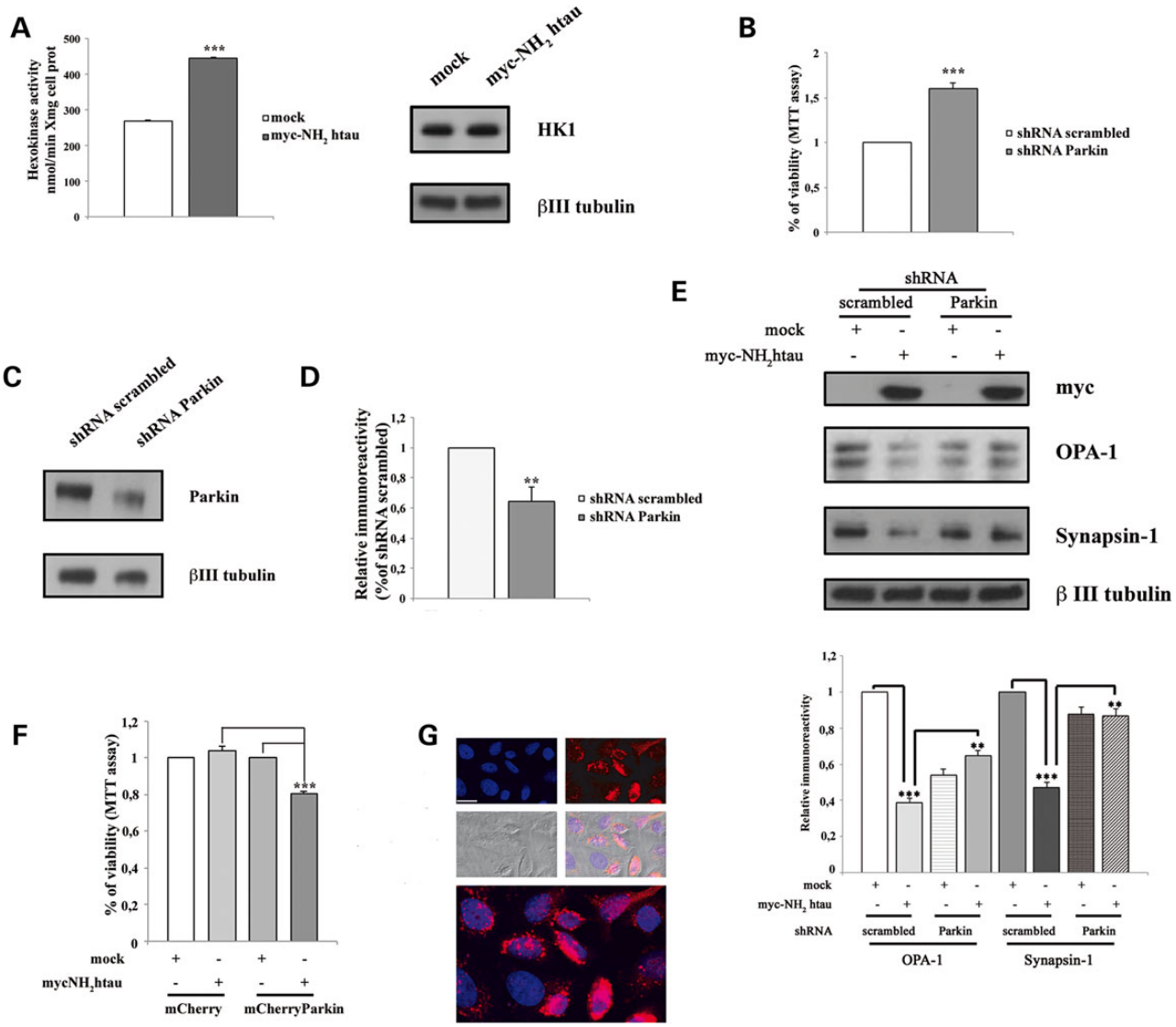

Figure 2. Parkin is involved in the NH_2htau-induced mitochondrial removal (**A**) Spectrophotometric determination of activity (expressed as % of control) of hexokinase (HK1), was assayed through a coupled reaction with glucose-6-phosphate dehydrogenase (G6PDH), following the NADP reduction at 340 nm ($\varepsilon_{340\,nm} = 6.22\ mM^{-1}\ cm^{-1}$). Absorbance was recorded with a Jasco doublebeam/double-wavelength spectrophotometer UV-550 and was normalized to the total proteins content of whole-cell homogenates from mock- or NH_2htau-tranduced neurons (MOI50) at 16 h post-infection (for detail see Materials and Methods). Values are means of five independent experiments and statistically significant differences were calculated by unpaired two-tailed Student's *t*-test (***$P < 0.0001$ versus mock). Western blotting analysis on total protein extracts from hippocampal primary neurons (DIV 15) infected with myc-NH_2htau (MOI 50) or with mock control (MOI 100) for 16 h shows no difference in cellular HK1 amount. β-III tubulin was monitored as loading control. (**B–E**) In (B) Hippocampal neurons were transfected by Nucleofector kit (AMAXA) with target-specific Parkin shRNA plasmid (shRNA Parkin) or with scrambled plasmid (shRNAscrambled), used as negative control. After 48 h, cultures were infected with myc-NH2htau (MOI 50) and with mock control (MOI 100) and viability was assessed by MTT assay at 16 h post-infection. The histogram reports the neuronal survival calculated as the ratio of respective myc-NH_2htau/mock values in shRNA Parkin-treated samples over the corresponding ones in shRNAscrambled-treated controls. Values are means of three independent experiments and statistically significant differences were calculated by unpaired two-tailed Student's *t*-test (***$P < 0.0001$ versus shRNAscrambled). In (C and D) Suppression of Parkin expression in neuronal cultures was validated at 48 h by western blotting analysis on total proteins extracts (C) and down-regulation in expression levels of protein was quantified by densitometry normalizing on β-III tubulin signal (D). Values are means of three independent experiments and statistically significant differences were calculated by unpaired two-tailed Student's *t*-test (**$P < 0.01$ versus shRNAscrambled). In (E) western blotting analysis ($n = 3$) on total protein extracts from hippocampal primary neurons transfected for 48 h with shRNAParkin plasmid or with shRNAscambled one and then infected with myc-NH_2htau (MOI 50) and with mock control (MOI 100) for additional 16 h. Immunoblots were probed with specific antibodies against mitochondrial and synaptic markers, such as OPA-1 and synapsin I, respectively. The exogenous expression of myc-NH_2htau was unchanged by treatments and densitometric quantification of immunoreactivity levels were calculated by normalizing the values on the β-III tubulin intensity. Values are means of three independent experiments and statistically significant differences were calculated by unpaired-two tailed Student's *t*-test (***$P < 0.0001$ versus mock; **$P < 0.01$ versus shRNAscrambled). Note that Parkin knockdown attenuated the loss of mitochondrial and synaptic content in NH_2htau-expressing group. (**F** and **G**) HeLa cells were 48 h transfected with plasmid expressing mCherry alone, as internal control, or with mChrerryParkin and then infected with myc-NH_2htau (MOI 50) and with mock control (MOI 100). Viability was examined at 16 h post-infection by MTT assay (F). Values are means of three independent experiments and statistically significant differences were calculated by unpaired two-tailed Student's *t*-test (***$P < 0.0001$). Note that ectopic introduction of Parkin-coding expression vector into HeLa cell-type restored mitochondrial vulnerability to NH_2htau-induced injury. Confocal microscopy analysis (G) on HeLacells transfected for 48 h with mCherry Parkin (red channel) was performed to check the successful delivery of exogenous transgene. Nuclei (blue channel) were stained with DAPI. A DIC (differential interference contrast) light transmitted channel was acquired to visualize the whole-cell morphology. Scale bar: 10 μm.

mitophagy in neurons (52,53,98,107), also displayed that a considerable amount of UCHL-1 was enriched in mitochondria from NH_2htau-expressing neurons. Remarkably, although UCHL-1 staining appeared in control neurons essentially cytoplasmatic and distributed to different subcellular domains, several UCHL-1-positive puncta colocalized with fragmented and circle-shaped mitochondria accumulating into the somatoneuritic compartment (mito-aggresomes) in NH_2htau-expressing neurons (Fig. 3B and B′ arrows). However, this distribution pattern ranged within different intensity degrees in number and size of colabeled dots (yellow) in clear association with the healthy state of neurons, suggesting that UCHL-1 mitochondrial localization was directly related to cellular damage. In detail, viable neurons showed neither fragmented mitochondria nor dystrophic neuritis and UCHL-1 homogeneously compartmentalized both in processes and cell body, in line with previous findings (61). Conversely, in dying neurons, dense clusters of round-shaped structures, which were both positive for UCHL-1 and mitochondrial markers (arrows), segregated into the somatic compartment mainly in perinuclear region, in a way which is similar to that is evident during canonical mitophagy in primary neurons (52,53). On the contrary, mock-infected neurons displayed a healthy and uniformly distributed Tomm20-positive mitochondrial network along with a more disperse and not-compartmentalized UCHL-1 staining in the cytoplasm, consistently with its physiological regular expression at synapses, soma and neuritis in cultured hippocampal neurons (60,61,108).

We subsequently tested our hypothesis that UCHL-1 and Parkin might colocalize at mitochondria in NH_2htau-expressing neurons, suggesting a potential functional interaction between these two proteins *in vitro*. Consistently with our biochemical and morphological data (Fig. 3A and B) and with tandem affinity purification/mass spectrometry (TAP)/MS) results by others (69,70), confocal analysis performed on 16 h-infected hippocampal cultures (MOI 50) following double immunofluorescence with UCHL-1 (green) and Parkin antibodies (red) revealed that an increased staining in UCHL-1-positive dots, which were also Parkin-labeled (yellow) and mainly distributed into the somatic perinuclear area (Fig. 3C′, arrows), was strongly noticeable after NH_2htau overexpression, again resembling the distribution of roundish and damaged mitochondria detectable during the explicit induction of selective mitophagy in neurons (52,53). Remarkably, this co-distribution pattern was also strictly reminiscent of the one described above (UCHL-1/mitochondrial markers, Fig. 3B and B′), suggesting that at least part of those UCHL-1/Parkin positive spots were mitochondria. Conversely, a diffuse and essentially not-overlapping cytoplasmatic pattern of UCHL-1 and Parkin was detected in mock-infected neurons. Interestingly, a comparable dotted co-staining pattern was also observed under the same experimental conditions in NH_2htau-dying neurons undergoing mitophagy but not in mock-infected cultures after double immunofluorescence staining for exogenous myc-tau (green) and Parkin (red) antibodies (Fig. 3C, arrows), suggesting that those Parkin-labeled punctate structures were also positive for truncated tau (yellow) and that at least part of them might be also positive for UCHL-1. Taken together these morphological data strongly suggest that UCHL-1, Parkin and myc-NH_2htau coexist at compromised spherical mitochondria in degenerating neurons, in line with our *in vitro* results from biochemical cytosol/mitochondria fractionation (Fig. 3A, 80) and with *in vivo* observations showing that NH_2htau specifically interacts with ruptured and disorganized mitochondria in human AD conditions (18,74,77).

Next, in order to confirm the effective role of UCHL-1 in removal of dysfunctional mitochondria in NH_2htau-dying neurons, we tested whether partial loss of UCHL-1 was *per se* able to rescue the detrimental tau-induced mitophagy and, then, cell viability in our 16 h-infected hippocampal cultures. As shown in Figure 3D by MTT assay at 16 h post-infection (MOI 50), neuronal death was significantly but partially relieved in NH_2htau-expressing cultures if neurons were formerly transduced with specific shRNA plasmid knock-downing the UCHL-1 expression (48 h before) but not with non-target shRNA (shRNAscrambled) one (Fig. 3E and F), in line with previous evidence showing that the suppression of UCHL-1 activity can provide different outcomes under normal versus pathological conditions in the context of α-synuclein-induced neurodegeneration (108). Remarkably, as shown by western blotting with OPA-1 and synapsin I (Fig. 3G), the downregulation of UCHL-1, which is moderately harmful in control group (108), restored the mitochondrial as well as synaptic protein content in tau-transduced neurons, just resembling the protective role afforded in these *in vitro* model by partial suppression of Parkin (Fig. 2B–E). Finally, no change in the protein levels of myc-NH_2htau was detected after shRNA treatment of neuronal cultures up to 48 h, ruling out the possibility of off-targets effects responsible of increased viability.

Remarkably, the physiological full-length human myc-tau 1–441 (htau40), which we reported does not change neither the viability (71), nor the estimation of mtDNA content or the expression levels of proteins involved in the mitochondrial autophagy as well as in the synapses stability (80), when overexpressed in neuronal cultures for 16 h and at similar low levels (MOI 50) of toxic NH_2htau fragment, was also unable to alter the cytoplasmatic distribution of both Parkin and UCHL-1 (Supplementary Material, Fig. S2), confirming again that the *in vitro* effects of NH_2-truncated tau are specific.

Taken together and in line with other papers reporting that abnormal and deleterious binding of UCHL-1 to several subcellular sites such as lysosomes (109,110) and endoplasmic reticulum (ER) (111) promotes the α-synuclein- induced neurotoxicity, our findings show that: (i) in NH_2htau-expressing neurons undergoing mitophagy, a stable proportion of UCHL-1 relocalizes to mitochondria and likely physically interacts with Parkin and exogenous myc-NH_2htau fragment; (ii) the deficiency of UCHL-1, as well as of Parkin, acts as a protective modifier against the NH_2htau-dependent *in vitro* neuronal death, by relieving autophagic mitochondrial loss and synapses demise.

Recruitment of UCHL-1 to mitochondria is also detected in human AD brains as well as in transgenic AD mice model

Increasing evidence has demonstrated that synaptic mitochondria of hippocampal and cortical regions from human AD specimens and presymptomatic (6-month-old) Tg2576 mice, a well-established AD animal model carrying the Swedish mutant form of Aβ precursor protein (AβPP), are more impaired than non-synaptic ones in their morphology, metabolic functions and quality control (8,32,112–115). In view of these considerations, we investigated whether the mitochondrial targeting of endogenous NH_2htau fragment, which we previously described to take place in vivo at synapses from human AD brains (17,77), is accompanied by a parallel redistribution of Parkin and UCHL1 to these organelles, in AD subjects as well as in Tg2576 transgenic mice.

To this aim, purified synaptosomal preparations, which represent ‘pinched-off nerve endings’ containing complete presynaptic terminals, mitochondria and synaptic vesicles along with postsynaptic membrane and postsynaptic density (PSD)

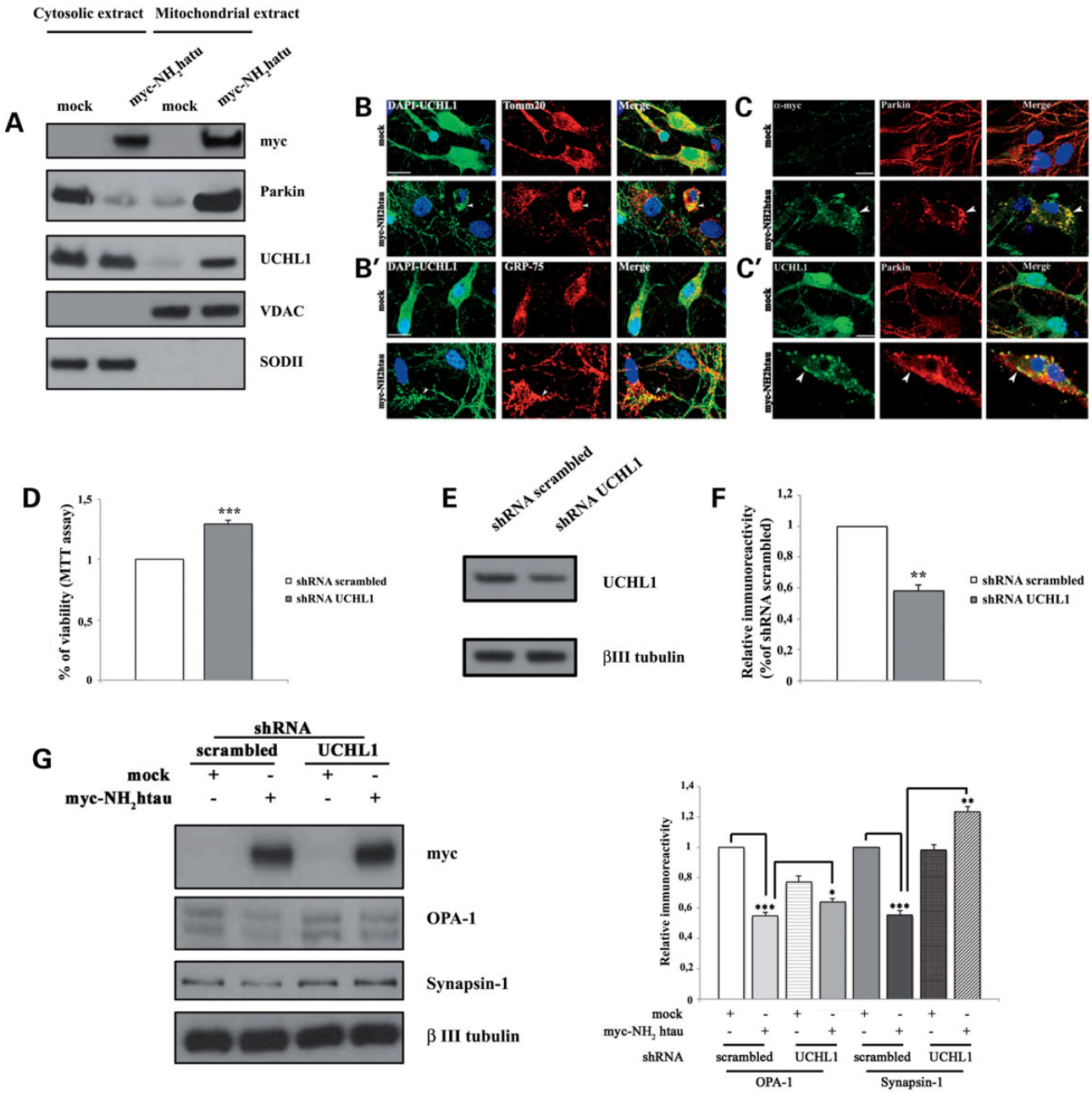

Figure 3. UCHL1 relocalizes to mitochondria in NH2htau-expressing neurons and participates to their deregulated autophagic clearance. (**A**) Western blotting analysis ($n = 3$) was carried out on equal proteins amount of cytosolic and mitochondrial fractions (40 μg) from hippocampal primary neurons (DIV15) adenovirally transduced for 16 h with myc-NH_2htau (MOI 50) or with mock control (MOI 100). Immunoblots were probed with antibodies against myc-tag (clone 9E10), Parkin (clone Park8) and UCHL-1(clone31A3) to show the co-distribution of overexpressed myc-NH_2htau with endogenous Parkin and UCHL-1 at mitochondria in infected neurons. The efficiency and the purity of mitochondrial preparation was checked by probing fractionated protein fractions with several specific antibodies reacting with cytoplasmatic (copper/zinc-Cu/Zn-SODI) and mitochondrial markers (VDAC). (B and B′) Confocal microscopy analysis of double immunofluorescence for UCHL-1 (green channel) and for two mitochondrial markers such as Tomm20 (red channel); (**B**) and GRP75 (Glucose-regulated protein 75) (red channel; (B′) carried out on primary hippocampal cultures at 16 h post-infection with mock- or with myc-NH_2htau-vectors (MOI 100-50, respectively). Nuclei were stained with DAPI (blue channel). Note that UCHL-1-positive, round-shaped and fragmented mitochondria (arrows) were mainly clustered in somatoneuritic regions of NH_2htau-expressing neurons while a more uniform network of interconnected organelles, along with a diffuse and not-overlapping cytoplasmatic pattern of UCHL-1, were clearly detectable in healthy control cultures.Scale bar: 10 μm. (**C** and C′) In C:Confocal microscopy analysis of double immunofluorescence for myc-tag (green channel) and for endogenous Parkin (red channel) carried out on primary hippocampal cultures at16 h post-infection with mock- or with myc-NH_2htau-vectors (MOI 100-50, respectively). Nuclei were stained with DAPI (blue channel). In (C′) Confocal microscopy analysis of double immunofluorescence for endogenous UCHL-1 (green channel) and Parkin (red channel) carried out on primary hippocampal cultures at16 h post-infection with mock-and myc-NH_2htau-vectors (MOI 100-50, respectively). Nuclei were stained with DAPI(blue channel). Note that in the NH_2htau-expressing neurons several UCHL-1 positive dots were also Parkin-labeled (yellow, arrows) resembling the co-distribution of UCHL-1/mitochondrial markers shown in B-B′. Scale bar: 10 μm. (**D–G**) In (D), hippocampal neurons were transfected by Nucleofector kit (AMAXA) with target-specific UCHL-1 shRNA plasmid (shRNA UCHL-1) or with scrambled plasmid (shRNAscrambled) used as negative control. After 48 h, cultures were infected with myc-NH_2htau (MOI 50) and with mock control (MOI 100) and viability was assessed by MTT assay at 16 h post-infection. The histogram reports the neuronal survival calculated as the ratio of respective myc-NH2htau/mock values in shRNA UCHL-1-treated samples over the corresponding ones in

(116), were first obtained from hippocampal regions of AD and age-matched cognitively intact human controls (ND). Human isolated nerve terminals were then analyzed by western blotting with CCP-NH_2 tau antiserum (Caspase-Cleaved Protein-NH_2tau antibody 26–36 residues), recognizing the endogenous 20–22 kDa NH_2h fragment without any cross-reaction with intact human full-length tau (17,74), with Parkin and UCHL-1 antibodies. Consistently with our *in vitro* results of ectopic overexpression of neurotoxic myc-NH_2htau (Fig. 3A), biochemical partition of cytosolic/mitochondrial proteins carried out on synapses-enriched fractions revealed that the elevated levels of endogenous 20–22 kDa NH_2htau distributed in AD mitochondria in correlation with a prominent immunoreactivity of Parkin (Fig. 4A, Supplementary Material, Fig. S3). Interestingly and in line with our previous investigations (77), we confirmed that the NH_2htau fragment ran on SDS–PAGE as a doublet with an additional faster band which stood constantly excluded from mitochondria being mainly recovered in corresponding cytoplasmic fraction (Fig. 4A, Supplementary Material, Fig. S3), likely due to its unknown post-translational modification such as monoubiquitylation which has been proved to critically govern the subcellular localization of Parkin and control its activation and/or translocation during induction of canonical mitophagy (103–105). Moreover, a sizeable amount of UCHL-1 (Fig. 4A, Supplementary Material, Fig. S3) was also recovered in mitochondrial fraction from synapses-enriched diseased samples in differently analyzed human brains, consistently with proportionally higher expression levels of NH_2htau associated with AD specimens than those derived from control ones.

Next the potential co-expression of NH_2htau, Parkin and UCHL1 at synapses was also assessed in cortical regions of Tg2576 mice (6-month-old) in comparison with their wt littermates. In order to detect early pathogenic changes in mitochondrial functions, which precede in this AD mice model the cognitive deterioration and Aβ aggregation starting at approximately six months of age (117), our synaptosomal preparations were also stained for red-fluorescent dye Mitotracker CMxRos (membrane potential-dependent) before performing the standard immunofluorescence procedures. Relevantly, accumulation of this functional probe into the lipid environment of mitochondria is driven in live cells by their membrane potential thus its fluorescence intensity indirectly indicates the energetic state of these organelles, allowing us to selectively probe synaptosomes endowed with still metabolically active mitochondria prior to overt neurodegeneration (7). Confocal microscopy of triple fluorescence for NH_2htau/Mitotracker/Parkin or NH_2htau/Mitotracker/UCHL-1 (Fig. 4B, lower and upper panels, respectively, of each experimental group) revealed that in presymptomatic Tg2576 mice a large proportion of stained synaptosomes co-expressed high levels of NH_2htau and Parkin or UCHL-1 mainly at mitochondria (Fig. 4B, arrows). At variance, in wt mice, NH_2htau exhibited low/very low basal staining and never colocalized with Parkin which displayed a not-preferential both cytoplasmic and mitochodrial distribution. Likewise, a significant colocalization of UCHL-1 and NH_2htau in synaptosomal mitochondria was not clearly detectable in not-transgenic healthy mice.

In order to better charactherize the actual sublocalization of these three proteins into synaptic compatments, we performed an additional extraction procedure on our purified synaptoneurosomes, by separating the Triton X-soluble fraction and PSD pellet which still retain synaptophysin and PDS95 markers, respectively (Fig. 4C). At our surprise but consistently with recent reports indicating that pathogenetic soluble tau species also exhibit a presynaptic localization (118) causing thus defective changes in probability of neurotransmitter release in P301L mutant human tau mice (119), we found that pathogenetic NH_2htau was distributed mainly into presynaptic fraction of both Tg and not-Tg mice showing an immunoreactivity which is much greater in unhealthy animals than in their control littermates. Besides, the immunoreactivity of NH_2htau fragment appeared as a doublet only in presynaptic but not in postsynaptic samples, suggesting that the unknown disease-associated transition from cytosplamatic to mitochondrial pathogenetic truncated tau started and/or took place for the most part in this specific subsynaptic regions, in line with the *in vivo* trans-synaptically spreading of tau pathology (120). Besides, UCHL-1 remained largely in presynaptic fraction, in agreement with the fact that only a slight subpopulation of active protein is distributed to spines and postsynaptic densities in neurons (61), while the proportion of Parkin displayed no significant difference by comparing the two synaptic subfractions in both blot profiles from Tg2576 and not-Tg mice.

On the whole, our results show that a significant co-enrichment and colocalization of endogenous NH_2htau fragment, UCHL-1 and Parkin, occur at mitochondria *in vivo* in both transgenic AD mice and AD brains, as we found in *in vitro* conditions (Fig. 3), and provide a hint that the pathogenetic accumulation of truncated tau may serve as docking site by stably sequestering UCHL-1 and Parkin on these organelles through physical anomalous protein–protein interaction.

Endogenous NH_2htau interacts with Parkin and UCHL-1 in human synaptic mitochondria from AD but not from age-matched cognitively intact controls

Having established that a proportion of UCHL-1 relocalized to mitochondria and plays a critical role in Parkin-dependent mitophagy in NH_2htau-dying cultured neurons, we addressed whether its anomalous interaction and/or co-distribution with endogenous mitochondria-targeted NH_2htruncated tau (17,74,77) and Parkin also took place *in vivo*, in human AD tissues. To this aim, co-immunoprecipitation (coIP) experiments on mitochondria-enriched fractions from hippocampal synaptosomes of AD and age-matched, not-demented (ND) specimens were performed using

shRNAscrambled-treated controls. Values are means of three independent experiments and statistically significant differences were calculated by unpaired two-tailed Student's *t*-test (***$P < 0.0001$ versus shRNAscrambled). In (E and F) knockdown of UCHL-1 in neuronal cultures was monitored at 48 h by western blotting analysis on total proteins extracts to assess the expression levels of target protein (E) and efficiency of gene silencing was quantified by densitometry normalizing on β-III tubulin intensity (F). Values are means of three independent experiments and statistically significant differences were calculated by unpaired two-tailed Student's *t*-test (**$P < 0.01$ versus shRNAscrambled). In (G) representative immunoblot ($n = 3$) of whole-cell lysates from hippocampal primary neurons transfected for 48 h with shRNAUCHL-1 plasmid or with shRNAscambled one and then infected with myc-NH_2htau (MOI 50) and with mock control (MOI 100) for additional 16 h by probing with specific antibodies against mitochondrial and synaptic markers, such as OPA-1 and synapsin I, respectively. The exogenous expression of myc-NH_2htau was unchanged by treatments and densitometric quantification of immunoreactivity levels were calculated by normalizing the values on the β-III tubulin intensity, used as loading control. Values are means of three independent experiments and statistically significant differences were calculated by unpaired two-tailed Student's *t*-test (***$P < 0.0001$ versus mock; **$P < 0.01$ versus shRNAscrambled; *$P < 0.05$ versus shRNAscrambled). Note that *in vitro* inhibition of UCHL-1 expression protects against NH_2htau-induced mitochondrial removal and synapses loss.

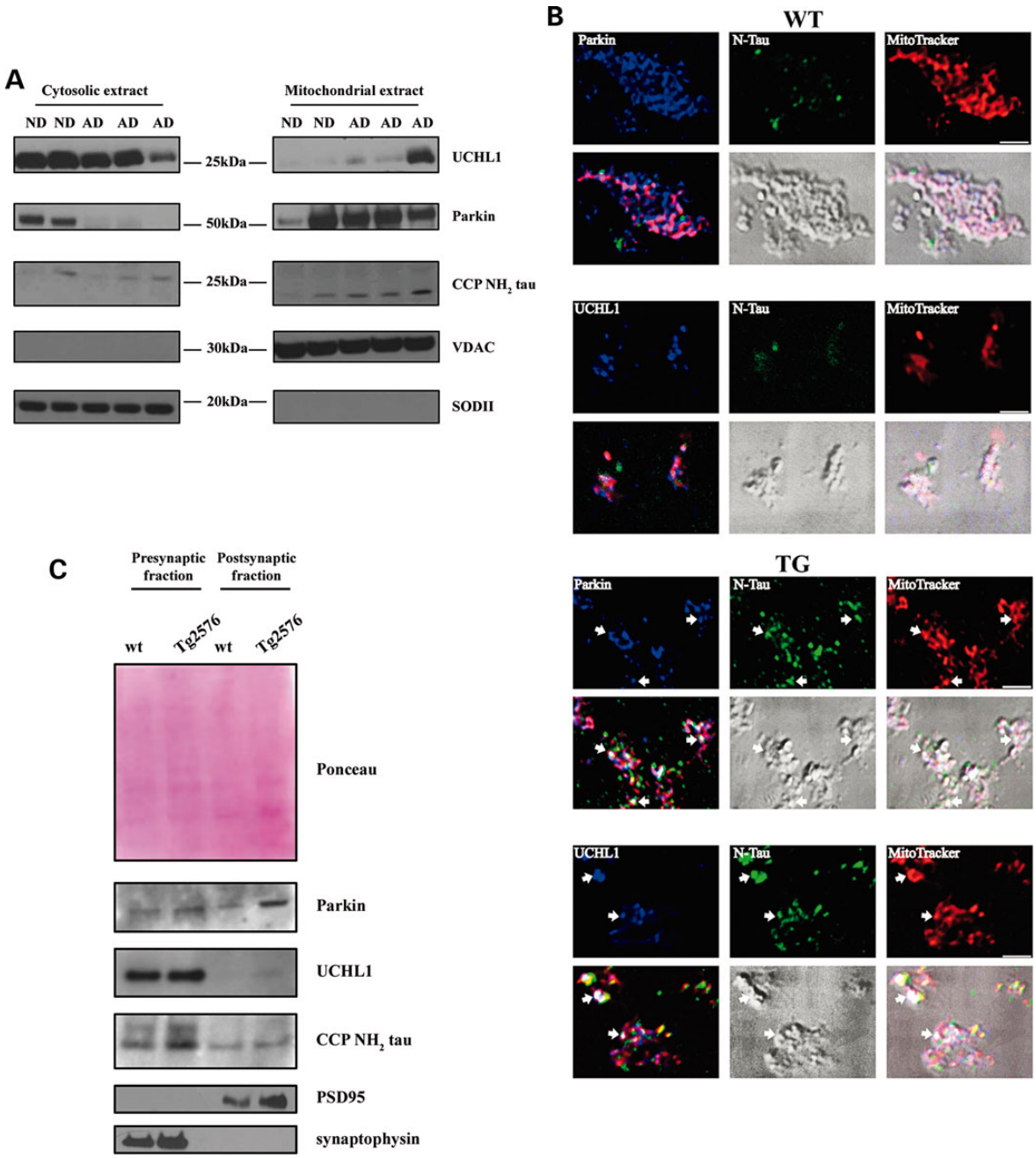

Figure 4. The endogenous pathogenetic NH_2-derived 20–22 kDa tau fragment, Parkin and UCHL-1 co-segregate in synaptic mitochondria from human AD cases as well as from Tg2576 AD mice (6-month-old). (**A**) The co-distribution of endogenous NH_2-derived 20–22 kDa tau fragment, Parkin and UCHL-1 in mitochondria was ascertained by western blotting analysis comparing equal proteins amount of cytosolic and mitochondrial fractions (25 μg) from purified synaptosomes of AD (AD) and age-matched, cognitively intact, not-demented (ND) human subjects. Immunoblots were probed with CCP-NH_2 tau (NH_2 aa2636 of human tau) antiserum recognizing the endogenous 20–22 kDa NH_2h fragment without any cross-reaction with intact human full-length tau (17,74), or with Parkin (clone Park8) or with UCHL-1 (PGP9.5 clone 31A3) antibodies. The efficiency and the purity of mitochondrial preparation was checked by probing fractionated protein fractions with several specific antibodies reacting with cytoplasmatic (copper/zinc-Cu/Zn-SODI) (D) and mitochondrial markers (VDAC). (**B**) Confocal analysis of triple colocalization in synaptosomes from cortical regions of Tg2576 mice (6-month-old) labeled with CCP-NH_2 tau antiserum (green channel), MitoTraker Red (red channel) and with Parkin (blu channel) or with UCHL-1 (blu channel). Panel shows fluoresecence single channels and fluorescence merge, DIC channel, fluorescence and DIC channel merge. Note that in synaptic mitochondria from Tg2576 mice, the endogenous NH_2htau fragment shows high expression levels and colocalization degree with either Parkin or UCHL-1 (arrows pointing to white dots which result from the merge of the three colours). Moreover, a proportion of NH_2htau fragment targets mitochondria without Parkin of UCHL-1 (yellow dots which result from the merge of the two colours, green and red) whereas its extra-mitochondrial staining (see above in (A) is also detectable (green dots), in line with our previous investigantions (77). Conversely, in litteramate not-Tg mice, the lower basal expression levels of NH_2htau expression do not show any appreciable colocalization pattern with either Parkin or UCHL-1. Scale bar: 3 μm. (**C**) Biochemical distribution of endogenous NH_2-derived 20–22 kDa tau fragment, UCHL-1 and Parkin in synaptosomal subfractions from cortical regions of Tg2576 (6-month-old) and littermate WT mice. Purified synatoneurosomes were further separated into the Triton X-extractable fraction and the crude PSD pellet, as shown by corresponding expression of synaptophysin and PSD95 markers. Western blotting analysis was carried out on equal amount of synaptosomal subfractions and Ponceau staining was used as loading control. Immunoblots were probed with CCP-NH_2 tau, mAb Parkin and UCHL-1. The high expression levels of NH_2htau in diseased AD mice are largely recovered in presynaptic fractions and co-segregate with Parkin and UCHL-1 in the same subcellular compartment.

as bait-antibody the CCP-NH_2 tau antiserum (Caspase-Cleaved Protein-NH_2tau antibody 26–36 residues) recognizing the endogenous 20–22 kDa NH_2h fragment without any cross-reaction with intact human full-length tau (17). As shown (Fig. 5B) by immunoblotting with a monoclonal detection-antibody against Parkin (clone Park8), a detectable proportion of endogenous Parkin co-imunoprecipitated with the NH_2htau fragment from AD mitochondria suggesting that an intact Parkin/NH_2htau complex was stably present in diseased neurons. Consistently with the undetectable or low/very low intracellular levels of NH_2htau fragment in physiological conditions, no comparable Parkin signal was co-immunoprecipitated by ND synaptic mitochondria. Control experiments demonstrated that NH_2htau fragment was efficiently enriched from mitochondria by IP with the respective antibody (Fig. 5A) and no signal was found when the bait-antibody CCP NH_2tau was replaced by preimmune IgG (not shown). Likewise, a small fraction of UCHL-1 was also co-immunoprecipitated with the NH_2htau fragment from AD mitochondria but not from control ones (Fig. 5C), showing that a trimeric NH_2htau/Parkin/UCHL-1 may exist only in pathological conditions whereas it appeared to be virtually excluded from not-diseased cases.

Reciprocal IP, carried out with the UCHL-1 capture-antibody followed by western blotting detection with CCP-NH_2 tau antiserum, *in vivo* confirmed a stable UCHL-1/NH_2htau physical interaction in AD mitochondria (Fig. 5F). Likewise and in line with our results of biochemical subcellular fractionation (Fig. 4A), Parkin co-immunoprecipitated together with UCHL-1 but only in AD-affected mitochondria-enriched fractions (Fig. 5E), confirming thus that the pathological high levels of mitochondria-targeted NH_2-htau fragment (17) was able to intercept and trap both UCHL-1 and Parkin on these organelles. Control experiments were performed to check that endogenous UCHL-1 protein was specifically and successfully immunoprecipitated by the respective antibody (Fig. 5D).

Next, as we carried out on tau-infected cultured neurons (Fig. 3B, B′, C and C′), we addressed morphological coexpression between endogenous NH_2htau/UCHL-1 and NH_2htau/Parkin by immunofluorescence experiments performed on brain tissues from AD and ND subjects. Confocal microscopy analysis on AD cerebral sections double-labeled with CCP-NH_2htau (green) and UCHL-1 (red) antibodies revealed a net increase in fluorescence intensity and number of co-labeled spots (yellow), akin to putative fragmented mitochondrial clusters surrounding degenerating and dysmorphic nuclei (Fig. 5L). Relevantly, in AD tissues (Fig. 5L, upper panel), the NH_2htau-positive puncta which were also strongly UCHL-1-labeled selectively concentrated into cell body whereas, in age-matched ND brains and in correlation with their faint expression levels of truncated tau (Fig. 5I upper panel), a more disperse and regular localization of UCHL-1 was detectable. Specific staining was lost by omission of CCP-NH_2 tau and UCHL-1 antibodies or by replacement of antibodies pre-adsorbed with their respective antigens or by preimmune IgG (not shown).

Quantitative analysis of the fluorescence intensity confirmed and extended our qualitative morphological observations (Fig. 5I–L, lower panel). In AD cases, the immunofluorescence intensity of NH_2htau and UCHL-1 significantly increased if compared with ND ones, reaching a percentage increase of 24 and 38%, respectively. For co-localization analysis, we took advantage of two different indexes, such as Pearson's and Manders' coefficients. The Pearson's coefficient in ND specimens was 0.34 ± 0.06 and in AD ones was 0.77 ± 0.03, accounting for a 94% significative increase (Student's *t*-test $^{*}P < 0.05$). In the ND conditions, the Manders' coefficients were 0.56 ± 0.06 for NH_2htau/UCHL-1 ratio and 0.72 ± 0.18 for UCHL-1/NH_2htau ratio. On the contrary, in AD, the Manders' coefficients were 0.67 ± 0.07 for NH_2htau/UCHL-1 ratio and 0.75 ± 0.05 for UCHL-1/NH_2htau ratio, accounting for only a modest and not significative 15% in the NH_2htau/UCHL-1 ratio but a 3% increase in the UCHL-1/NH_2htau ratio. The analysis of these two colocalization indexes pointed to a major and significative increase in the correlation (Pearson's) between the fluorescent signals, although a not significative increase in the fluorescence association ratio (Manders) was also detected.

Likewise, confocal microscopy analysis on human hippocampal sections double-labeled with CCP-NH_2 tau (green) and Parkin (red) antibodies displayed that NH_2htau-positive mitochondria were also decorated with endogenous Parkin in AD specimens (Fig. 5H, upper panel). Interestingly, both Parkin and NH_2htau appeared to be selectively concentrated into perinuclear and somatic compartments and co-localized only in fragmented and spherical dotted structures resembling mitochondria similar to those that we and others have previously described to be clearly detectable in primary neurons after frank mitophagy induction (17,52,53,98). Note that a tiny amount of NH_2htau was also present away from mitochondria into dystrophic neuritis (arrows), in line with previous immunohistochemistry studies referring an additional but less prominent subsynaptic, extra-mitochondrial distribution of the N-derived D25-cleaved human tau fragment(s) in AD brains (74,77). Conversely, a non-overlapping distribution was found in age-matched ND tissues which revealed a low intensity and a more diffuse immunostaining of Parkin being mainly localized in the cytosol or only occasionally dotted in line with an almost undetectable intracellular expression of NH_2htau (Fig. 5G, upper panel). Specific staining was lost by omission of CCP-NH_2 tau and Parkin antibodies or by replacement of antibodies pre-adsorbed with their respective antigens or by preimmune IgG (not shown).

Quantitative analysis (Fig. 5G and H, lower panel) showed that, in the NH_2htau/Parkin double-labeled sections, the NH_2-htau immunofluorescence intensity significantly increased in AD specimens of 18% in respect of ND ones, whereas the Parkin intensity significantly increased of 26%. The Pearson's coefficient in ND cases was 0.17 ± 0.18 and for AD ones was 0.70 ± 0.16, accounting for a significative 283% increase (Student's *t*-test $^{**}P < 0.05$). The Manders' coefficients were 0.73 ± 0.02 for NH_2-htau/Parkin ratio and 0.68 ± 0.07 for Parkin/NH_2htau ratio in ND conditions. In AD, the Manders' coefficients were 0.76 ± 0.12 for NH_2htau//Parkin ratio and 0.88 ± 0.17 for Parkin/NH_2htau/ ratio, accounting for a modest and not significative 2% in the NH_2-htau/Parkin ratio and a 4% increase in the Parkin/NH_2htau ratio.

Taken together, these qualitative and quantitative morphological data suggested that in age-matched ND cases the basal expression levels of NH_2htau were localized with either Parkin or UCHL-1 to the same subcellular domains (high Mander's coefficients) but these proteins were not highly compartmentalized and significantly correlated (low Pearson's coefficient; see also the Plot Profile). On the contrary, in the AD cases, the high expression levels of NH_2htau, UCHL-1 and Parkin were still localized to the same subcellular compartments (high Mander's coefficients) but, importantly, they were also highly compartmentalized and significantly correlated (high Pearson's coefficient; see also the Plot Profile).

Altogether our results indicate that: (i) an aberrant binding between the endogenous NH_2htau fragment, UCHL-1 and Parkin takes place only at diseased synaptic mitochondria in degenerating AD human neurons, as we detected in synaptosomes from Tg2576 AD animal model (Fig. 4B) and *in vitro* after ectopic expression of neurotoxic myc-NH_2htau (Fig. 3B and C); (ii) the

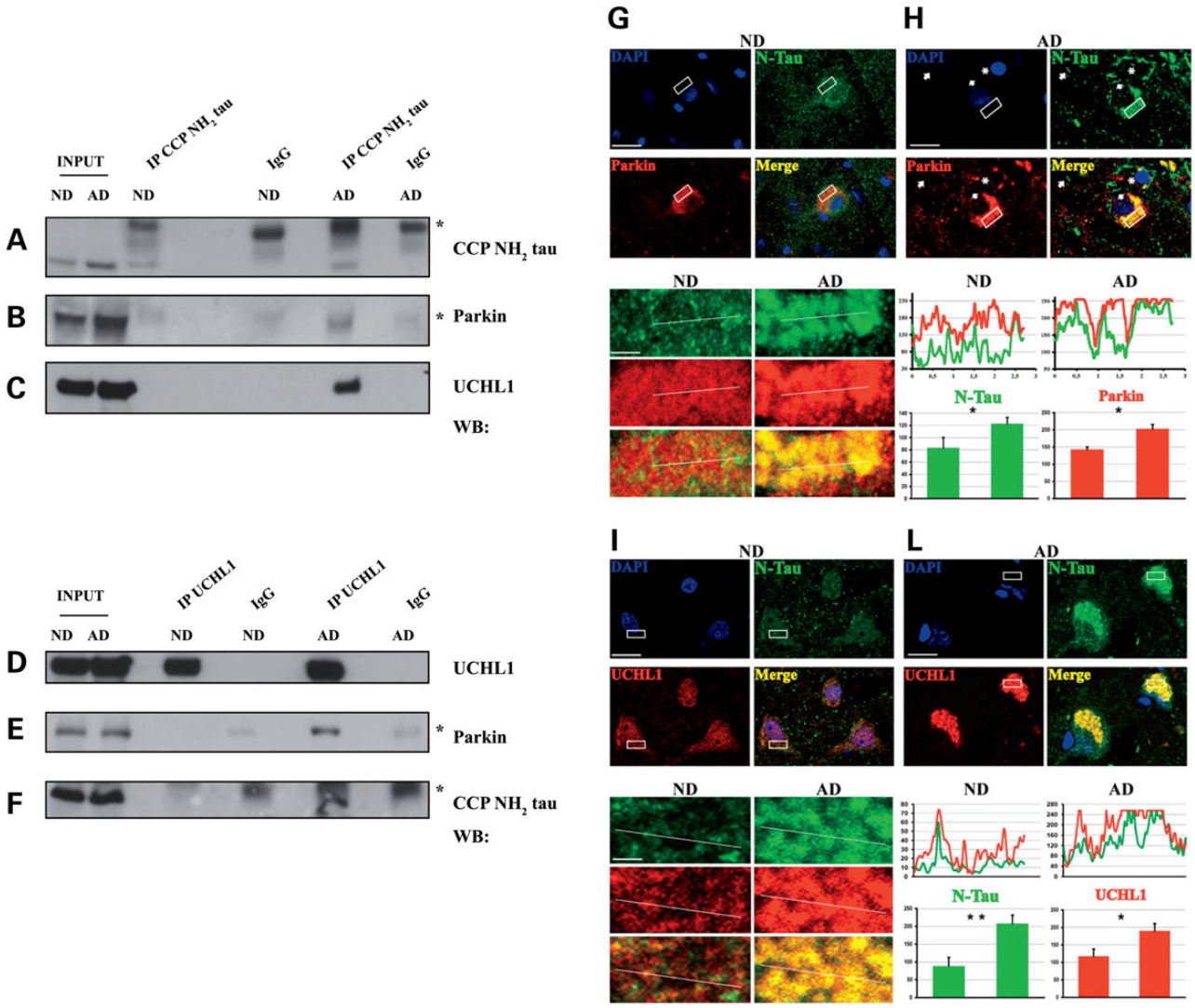

Figure 5. Endogenous NH_2htau stably interacts and colocalizes with Parkin and UCHL-1 in synaptic mitochondria from AD patients but not from age-matched cognitively intact controls (**A–C**). In (B and C) representative western blotting analysis ($n = 3$) comparing mitochondria-enriched extracts (500 μg) from ND and AD human synaptosomes immunoprecipitated (IP) with CCP-NH_2 tau (NH_2 aa26-36 of human tau) antiserum or IgG, used as negative control. Immunoblots were probed (WB) with Parkin (Park8 clone) (B) and UCHL-1 (PGP9.5 clone 31A3) (C) antibodies. Total proteins from ND and AD cases (20–25 μg INPUT) were also loaded for lane and included as positive internal control of electrophoretic mobility and IP enrichment. Asterisk indicates the signal of immunoglobulin heavy chains. No signal was found when the bait CCP-NH_2 tau antiserum was replaced by preimmune IgG. In (A) control experiments demonstrated the NH_2htau fragment around 20–22 kDa was efficiently immunoprecipitated with CCP-NH_2tau antiserum. Asterisk indicates the signal of immunoglobulin heavy chains. (**D–F**) In (E and F) mitochondrial fractions were purified from ND and AD synaptosomes and proteins (1 mg) were subjected to reciprocal IP with IP-suitable UCHL-1 antibody or IgG, used as negative control. Western blots shown were representative of at least three separate experiments and immunoblots were probed with Parkin (aa304-322 of Parkin) (E) and with CCP-NH_2 tau (NH_2 aa26-36 of human tau) antisera (F). No specific band corresponding to the signal of immunoglobulin heavy chains (asterisk) was found when the UCHL-1 bait-antibody was replaced by preimmune IgG. In (D) control experiments was carried out to ascertain the efficiency of IP performed using UCHL-1 bait-antibody. (**G** and **H**) Upper panel: confocal images of double immunofluorescence with polyclonal CCP-NH_2 tau (NH_2 aa26-36 of human tau, green channel) and mouse Parkin (Park8 clone, red channel) antibodies on hippocampal CA1 region from AD (H) and age-matched ND control case (G). Nuclear counterstaining was with DAPI (blue channel). In the control specimens, the Parkin immunoreactivity was largely diffuse in the cytoplasmatic domain—or occasionally dotted—while the CCP-NH_2tau staining appeared barely detectable on the tissue background, with the exception of several intense puncta, and did not show appreciable colocalization with Parkin. In the diseased subjects, the CCP-NH_2 tau as well as the Parkin staining intensities were more intense, highly colocalized, confined to putative fragmented and highly clustered mitochondria. Glial cells (asterisk)—which are easily distinguished by their compact nuclear area displaying an intense DAPI fluorescence—also exhibited low levels of Parkin immunoreactivity in ND cases compared with a more intense and clustered staining detectable in AD specimens. Note that there are several CCP-NH_2tau immunopositive structures resembling dystrophic neuritis (arrows) which are not Parkin immunoreactive. Lower left panel: inset boxes are high magnifications from AD and ND cells showing in detail the cytoplasmatic texture. Note the more diffuse appearance of both Parkin and CCP-NH_2tau immunoreactivity in ND cases, and the densely clustered immunoreactive nature of the cytoplasmatic texture in AD specimens. Lower right panel: image analysis performed on the cytoplasmatic texture. Top plots illustrate the intensity-distance (pixel/μm) profiles derived from inset boxes white line displaying for ND cases a rather homogeneous pixel intensities distribution endowed with a low-medium matching trend between the two analyzed channels which indicates the lack of signal colocalization. On the contrary, in AD specimens the intensities distribution displays alternating peaks and valleys suggestive of a patchy distribution endowed with a high- similarity trend between the two analyzed channels. Bottom histograms show the fluorescence intensities for CCP-NH_2 tau (green column) and for Parkin (red column). Immunofluorescence studies shown were representative of at least two separate experiments. Scale bars: upper panel = 10 μm and lower panel = 1 μm. (**I–L**) Upper panel: confocal images of double immunofluorescence with polyclonal CCP-NH_2 tau (NH_2 aa26-36 of human tau, green channel) and mouse UCHL-1 (PGP9.5 clone 31A3, red channel) antibodies on hippocampal CA1 region from AD (L) and age-matched ND control cases (I). Nuclear counterstaining was with DAPI (blue channel).

NH_2htau-dependent deleterious action on mitochondrial turnover can be *per se* a by-product of the overactivation of intracellular degradation machinery, likely due to improper engagement of Parkin and UCHL-1 to mitochondria which force these organelles to inappropriate or excessive elimination via selective autophagy (17,80).

Discussion

In the present paper, we extend our previous observations concerning the deregulated autophagic clearance of mitochondria triggered in post-mitotic neurons by the increased intracellular levels of toxic NH_2htau fragment (80), which *in vivo* prominently targets and affects mitochondria at AD synapses (17,77). Here, we show that: (i) the imbalanced Parkin-mediated mitophagy plays a pro-death role in our *in vitro* neuronal AD model; (ii) the NH_2htau fragment alters the quality control of neuronal mitochondria by facilitating subcellular trafficking and/or recruitment of both Parkin and UCHL-1 to these organelles making them more prone to indiscriminate and detrimental autophagic removal.

Unbalanced mitophagy is harmful in post-mitotic neurons

Several lines of evidence have confirmed a pathogenetic role of deregulated mitophagy in neurodegeneration, as a maladaptive and imbalanced response to pathological stressors (121). In post-mitotic neurons, which critically relies on mitochondria-derived ATP for their energetic demands, the ability of compensating an increased mitochondrial clearance with an appropriate biogenesis of these organelles plays a critical role in dictating the final outcome of adaptation/recovery from mitophagy-inducing injuries and cell survival (38). In fact, although the clearance of dysfunctional or damaged mitochondria is neuroprotective by preventing release of deleterious ROS and pro-apoptogenic factors or accumulation of toxic oxidative proteins, lipids and DNA, an excessive, inadequate or incomplete mitophagy, which is not properly balanced by coupled up-regulation in biogenesis of these organelles, can provoke in neurons a significant reduction in aerobic respiration due to net loss of functional and intact mitochondria (41) as well as degeneration of dendrites (122) leading, eventually, to cell death (39,40,86,123,124). To this regard, an increased autophagic turnover of mitochondria has been detected in injured AD neurons (25,28–31) and pathological tau *per se* can affect the mitochondrial quality control (18–20,80) as well as the autophagic pathway (125,126). In line with previous findings reporting that unbalanced mitophagy can be extremely deleterious in post-mitotic neurons (41,86,121,123), by complementary pharmacological and genetic approaches (Figs 1 and 2), we show a selective pro-death role of Parkin-dependent mitophagy in mature hippocampal neurons that ectopically express the toxic NH_2htau fragment, extending thus our previous observations which demonstrate that early changes in mitochondrial dynamics as well as mitochondrial recruitment of endogenous Parkin, bioenergetic deficits and synaptic damages strongly correlate with the extent of cell death in this *in vitro* AD model (80). Moreover, inhibition of excessive mitophagy in our NH_2htau-transduced neurons, although partially restores the mitochondrial content (Figs 2E and 3G), does not completely prevent the mitochondrial damage resulting in a modest but significant protection against the cell death assessed at 16 h post-infection (Fig. 1A). Consistently with our results, knocking down of Parkin by shRNA-encoding plasmids or overexpression of wtMfn2 are sufficient *per se* to suppress the excessive mitophagy occurring in A53T α-synuclein-expressing dopaminergic neurons, providing thus a partial but significant protection against cell death in this *in vitro* PD model (41). Interestingly and just resembling the deleterious role of pathogenetic NH_2htau fragment in *in vivo* AD conditions (17,77), mutant A53T α-syn also physically localizes to dopaminergic mitochondria *in PD transgenic mice* and impacts on their function and/or integrity, leading to respiratory complex I inhibition along with an increased mitophagy (127). Moreover, *in vivo* Parkin deficiency delays the progression of neurodegeneration in mice overexpressing mutant A30P α-synuclein (128,129), as well as Parkin-null cortical neuronal/glial cultures are more resistant than wild-type ones to toxicity of Aβ oligomers (130) that also target and impair AD mitochondria in cooperation with the pathogenetic tau (16,17,77). Taken together, our findings further strengthen the causal relationship between uncoordinated mitophagy and neurodegeneration (38), by identifying the deregulated clearance of mitochondria as one of the pathological changes *underlying synapses degeneration associated to* N-terminal truncation *of tau which* early *occurs in* diverse human age-related tauopathies including AD (4).

The protective versus toxic role of UCHL-1 and Parkin in AD neurodegeneration

Concerning the pathogenetic role of aberrant physical interaction between NH_2htau, UCHL-1 and Parkin in promoting extensive mitophagy, as we detected both *in vitro* and *in vivo* in synaptic mitochondria from human AD brains and pre-symptomatic Tg2576 transgenic mice (Figs 4 and 5), we wish to stress that these two enzymes can function in the context of neurodegeneration in opposite ways and change their physiological role in tight relation to cellular conditions, interaction with other regulatory proteins and/or post-translational modifications which control activity and substrate selectivity (131).

In fact, environmental and/or intrinsic factors can irreversibly compromise the well-known broad-spectrum protective functions ascribed to both UCHL-1 and Parkin by predisposing or accelerating vulnerability of neuronal populations to degeneration, in particular when they are challenged by chronic exposure to

In ND, the UCHL-1 immunoreactivity appeared uniformly expressed in both cell bodies and processes and did not merge with the CCP-NH_2 tau staining which was hardly detectable on the tissue background. Conversely, the increased signal intensity of CCP-NH_2 tau labeling was clearly detectable in AD samples and robustly colocalized with UCHL-1 immunoreactivity. Note that both stainings appeared dot-shaped and restricted to putative, compromised and spherical mitochondria accumulating in perinuclear sites. Lower left panel: inset boxes are high magnifications from AD and ND cells illustrating in detail the cytoplasmatic texture. In ND cases, the homogeneous and diffuse cytoplasmatic texture was only occasionally endowed with dots showing immunoreactivity for both UCHL-1 and CCP-NH_2 tau. On the contrary, in AD conditions, both UCHL-1 and CCP-NH_2 tau stainings display a cytoplasmatic texture characterized by a more densely clustered immunoreactivity and a high colocalization degree. Lower right panel: image analysis performed on the cytoplasmatic texture. Top plots illustrate the intensity-distance (pixel/μm) profiles derived from inset boxes white lines showing for ND cases a heterogeneous pixel intensities distribution endowed with a low-medium similarity trend between the two analyzed channels which indicates the essential lack of signal colocalization, with the exception of some rare dotted structures. In AD specimens, the intensities distribution exhibits alternating peaks and valleys suggestive of a patchy distribution characterized by a highly significative matching trend between the two channel curves. Bottom histograms display the fluorescence intensities for CCP-NH_2 tau (green column) and UCHL-1 (red column). Immunofluorescence studies shown were representative of at least two separate experiments. Scale bars: upper panel = 10 μm and lower panel = 1 μm.

cumulative insults such as those experienced by brain in slow and progressive age-dependent neurodegenerative diseases. To this regard, although a marked reduction in soluble form as well as in overall activity of UCHL-1 (65–68) has been speculated to contribute to familiar and sporadic AD pathogenesis, its *in vivo* genetic ablation in mice produces *gad* (gracile axonal dystrophy) phenotype which is characterized by 'dying-back'-type axonal degeneration with accumulation of APP, Aβ peptide(s) but devoid of any obvious neuronal loss and, more importantly, by a robust resistance to ischemic injury (132) or to accumulation of α-synuclein (133) which both are insults occurring during normal aging and mainly associated with induction of mitophagic signaling (127,134). Compelling *in vivo* evidence has also demonstrated that transduction of UCHL-1 as fusion protein into the hippocampus of APP/PS1 transgenic mice is beneficial, by restoring the normal activity of UPS which, in turn, stimulates in neurons the PKA/CREB (cAMP-dependent protein kinase (PKA)-cAMP response element binding protein) pro-survival pathway (63,64). Nevertheless, recent findings indicate that UCHL-1 *per se* does not significantly influence the activity of proteasome machinery because no detectable change in ubiquiting hydrolysis has been found *in vivo* after its genetic ablation (135,136). On the contrary, an alternative non-degradative role of UCHL-1 in the lysosomal pathway has been proposed, consistently with the findings that: (i) this multifunction enzyme also exhibits an ubiquitin ligase activity and, similarly to Parkin, is able to generate lysine (K)-63 linked side chains involved in proteasomal-independent signaling pathway (60); (ii) its pharmacological or genetic functional depletion leads to significant alterations in levels of cathepsin D and L lysosomal proteases, *in vitro* as well as *in vivo* (65,135). On the other hand, an unbalanced ubiquitin hydrolase and/or ligase activity acquired by 'gain-of-function' variants of UCHL-1 have also been suggested to critically participate to AD synaptic failure and neurodegeneration, as a consequence of its age-dependent oxidative post-translational modifications (67,137–140), its increased interaction with membranes (141) or its anomalous binding with other cellular partners such as Amyloid Precursor Protein (APP) (142). Actually, in AD brains, most of UCHL-1 variants are irreversibly and harmfully oxidized (68,138,140), display an increased insolubility and/or an elevated anomalous interactions with a variety of proteins resulting in deleterious effects on cellular physiology. For instance, an aberrant binding between UCHL-1 and tubulin and several membrane-bound lysosomal proteins, such as lysosome-associated membrane protein type 2A (LAMP-2A), heat shock cognate protein 70 (Hsc70) and heat shock protein 90 (Hsp90), has proved to adversely impinge on microtubule dynamics and on Chaperone-Mediated Autophagy (CMA) which is another form of selective but ubiquitin-independent autophagy, respectively (109,110). The identification of S18Y polymorphism in UCHL-1 gene, which in genetic-epidemiological studies appears to reduce susceptibility to AD (143), further supports the notion that an actual dysregulation of UCHL-1 plays an important role in AD neurodegeneration and that its functional loss may also have neuroprotective effects under several pathogenic conditions, providing thus beneficial effects on neuronal survival (60,108,133).

Likewise, although Parkin overexpression is generally considered neuroprotective in several tauopathies mainly by promoting the proteasome/ubiquitin-dependent degradation of misfolded aggregates of β-amyloid and phospho-tau (144–146), stressor-induced post-translational modifications, interactions with not-canonical binding partners and oxidation/S-nitrosylation have been proved to adversely change its biochemical and functional properties, harming thus neuronal survival by means of alterations in subcellular localization, solubility and/or enzymatic activity (147–154). Furthermore, emerging roles of ubiquitin and ubiquitin-binding proteins in selective Parkin-driven mitophagy have been recently highlighted (45) and UCHL-1 has been identified as a novel candidate Parkin-associated protein by TAP/MS proteomic approaches on human SH-SY5Y neuronal cells undergoing frank mitophagy after FCCP-provoked dissipation of $\Delta\psi_m$ (69,70). In this context and in line with intrinsic ability of UCHL-1 to control in *in vitro* and *in vivo* neurons the steady-state of ubiquitin pool by direct association with free monomer (58), we wish to point out that our results reveal a novel and causal autophagy-modifying role of this enzyme in promoting extensive turnover of mitochondria occurring in NH_2htau-expressing cultured neurons, as demonstrated by the fact that mitochondrial loss and cell death are partially but significantly relieved after *in vitro* genetic suppression of its expression by shRNA-encoding plasmid. Finally, our data showing a toxic gain-of-function of UCHL-1 in affecting Parkin-dependent mitophagy in NH_2htau-expressing neurons (Fig. 3) are also supported by recent results, demonstrating that the genetic and pharmacological suppression of UCHL-1 activity provoke opposite effects on synapses stability and autophagic pathway in not-transgenic versus α-synuclein overespressing transgenic mice since this enzyme can function in different ways under pathogenetic versus physiological conditions (108).

Concluding remarks

In conclusion, we provide new insights into gain-of-function mechanism(s) underlying NH_2htau-induced neurotoxicity at synapses, showing that this pathogenetic truncated form of tau, whose levels are increased in affected mitochondria from human AD brains (17,77), improperly sequesters Parkin as well as UCHL-1, compelling these organelles to inappropriate/excessive and deleterious elimination via selective autophagy. We propose that both Parkin and UCHL-1 may have a dual participation in the context of AD mitochondrial impariment and neurodegeneration and in relation to the expression threshold of toxic NH_2htau fragment (Fig. 6): (i) a protective role (i.e. in normal conditions when only low/very levels of NH_2htau fragment are present at mitochondria) by promoting in neurons the ubiquitin-dependent degradation of misfolded proteins and/or dysfunctional mitochondria as well as by controlling the general stability of intracellular pool of ubiquitin; (ii) alternatively a noxious role, by dictating the outcome for the activation of deleterious mitophagic pathway due to their anomalous interaction at mitochondria with the higher pathological levels of NH_2htau fragment .

Finally, our findings will contribute to better understand the actual role of mitochondrial dynamics and mitophagy in AD-associated, tau-dependent synaptic dysfunctions in order to proceed developing therapeutic strategies to treat this devastating disease.

Materials and Methods

Reagents and antibodies

Bafilomycin A1 (BAF-A1) B1793, 3-methyladenine (3MA) M9281, cloroquine (CQ) C-6628, Carbonyl cyanide 4-(trifluoromethoxy) phenylhydrazone (FCCP) C2759 were from Sigma Aldrich. Rapamycin, 553210 was from Calbiochem.

The following antibodies were used: β–III tubulin antibody rabbit ab18207 Abcam; Mfn2 antibody mouse ab56889 Abcam; anti-Flag (cloe M2) mouse F3165 Sigma-Aldrich; Myc(9E10)

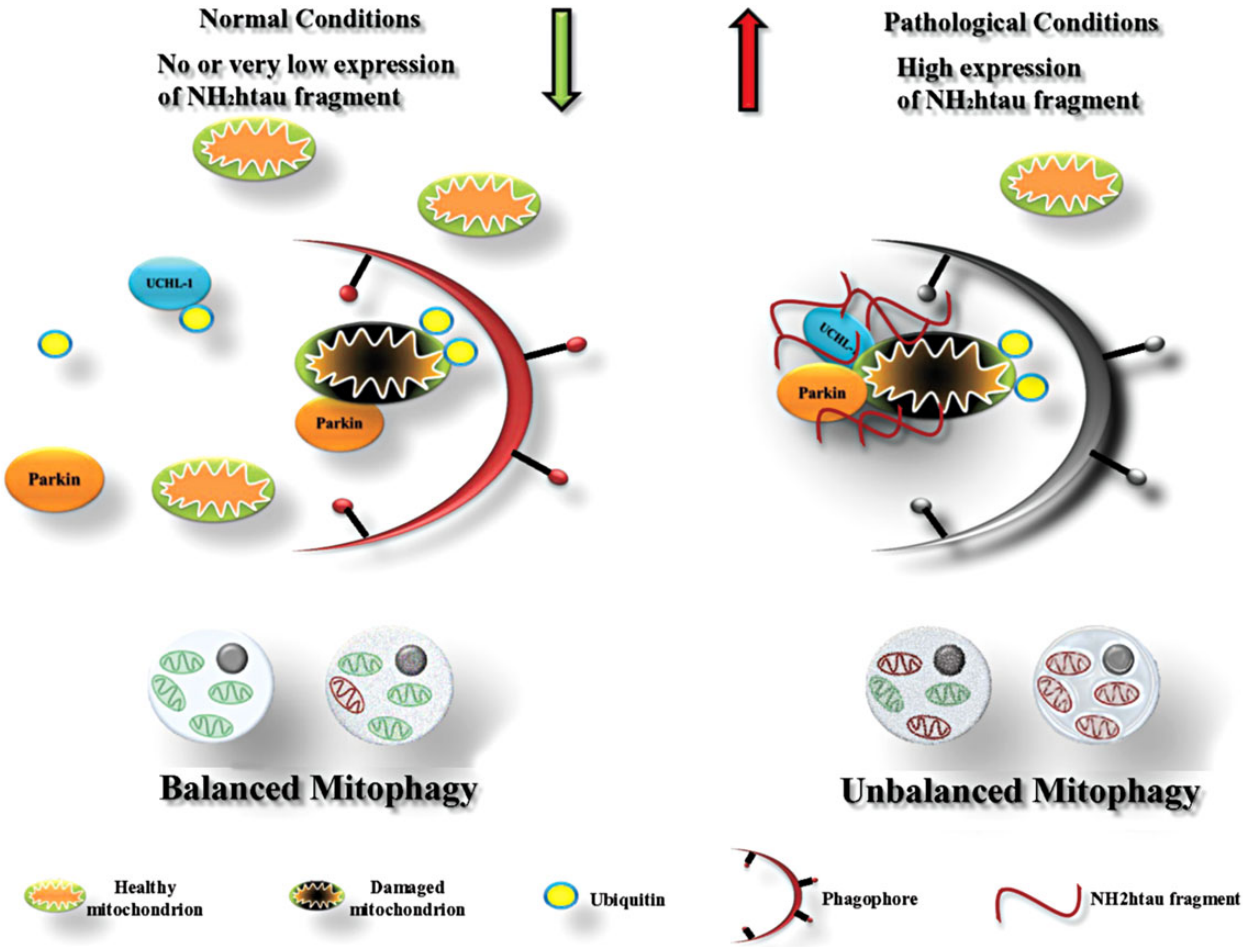

Figure 6. Proposed gain-of-function mechanism for detrimental regulation of mitochondrial clearance underlying NH_2htau-induced neurotoxicity. (**A**) In physiological conditions, the expression of NH_2h-truncated human tau at mitochondria in neurons is at low/very low levels. Parkin and UCHL-1 are required to maintain, directly or indirectly by controlling the steady-state levels of intracellular monoubiqutin, the balanced mitochondrial recycling as well as the normal cell function and survival. (**B**) In pathological conditions, the increased amount of toxic mitochondria-targeted NH_2htau fragment leads in neurons to formation of a triple complex by its aberrant interaction with Parkin and UCHL-1. The complex NH2htau fragment/Parkin/UCHL-1 overdrives autophagic clearance of mitochondria, resulting in 'mitophagic' neuronal death.

antibody mouse sc-40 Santa Cruz Biotechnology; c-Myc (A14) antibody rabbit sc-789 Santa Cruz Biotechnology; OPA1 antibody mouse 612606 BD Transduction Laboratories; Parkin antibody rabbit ab15954 Abcam; Parkin antibody mouse (clone Park8) P6248 Sigma-Aldrich; Synapsin I antibody rabbit AB1543P Millipore Corporation; SOD II (MnSOD, mitochondrial superoxide dismutase) rabbit SOD-110D Stressgen Biotechnologies; Tomm20 antibody rabbit (FL-145) sc-11415 Santa Cruz Biotechnology; Anti-VDAC/Porin antibody ab34726 Abcam; Anti-MFN2 (AB2) antibody rabbit AV42420 Sigma; PGP9.5 (clone 31A3) antibody mouse (MO25010) Neuromics; UCHL-1 antibody NBP1-49851 rabbit Novus Biologicals; UCHL-1 IP-specific antibody (EPR4118) NBP1-96612 rabbit Novus Biologicals; UCHL-1 antibody (C4) sc-271639 mouse santaCruz; UCHL-1 antibody 3524 rabbit Cell Signaling; Anti-HKI (C35C4) rabbit Cell Signaling; calpastatin antibody (clone PI11) MAB3084 mouse Millipore; PSD95 antibody (clone 7E3-1B8) mouse MAB1598 Millipore; synaptophysin antibody sc-17750 mouse Santa Cruz.

Brain material

Human brain material was provided via the rapid autopsy programme of the Netherlands Brain Bank (NBB), which provides post-mortem specimens from clinically well documented and neuropathologically confirmed cases. Tissue (hippocampus and superior frontal cortex) derived from Alzheimer disease (AD) cases and age-matched cognitively intact not diseased (ND) cases were used. For details (ethics statement declarations and subjects' demographics) see (17).

Cell culture and treatments

HeLa cells (American Type culture Collection, Rockville, MD, USA) were grown in DMEM medium (Invitrogen, Gibco BRL 41965-039) supplemented with 10% fetal calf serum (Invitrogen, Gibco BRL 10108-157), 100 U/ml of penicillin and 100 μg/ml of streptomycin (Invitrogen, Gibco BRL 15140-122) and maintained at 37°C in a saturated humidity atmosphere containing 95% air and 5% CO_2.

Hippocampal neurons were prepared from embryonic day 17–18 (E17/E18) embryos from timed pregnant Wistar rats (Charles River), as we previously reported (72). In detail, the hippocampus was dissected out in Hanks' balanced salt solution buffered with HEPES and dissociated via trypsin/EDTA treatment. Cells were plated at 1×10^6 cells on 3.5-cm dishes pre-coated with poly-D-lysine. After 2 days of culturing in neurobasal medium with B-27 supplement and glutamax, cytosine arabinofuranoside was

added to reduce glial proliferation. Half of the medium was changed every 3–4 days and mature neuronal cultures were infected at 15 days *in vitro*, as reported in (72). All experimental details concerning the handling with recombinant adenoviral vectors (construction, packaging, purification, titration), the used infection protocol, the time course of overexpression levels and the neuronal viability assays of both tau-coding and control transgenes have been previously reported in (71,72).

All animal experiments were approved by the CNR Animal Care and Use Committee and were conducted in full accordance with the Guide for laboratory animal practice with care to minimize the number of animals and their suffering.

Assessment of neuronal viability

Cell viability was quantified by counting the number of intact nuclei, after lysing in detergent-containing solution (155,156) and by the MTT tetrazolium salt assay (157).

DNA transfection

Hippocampal primary neurons were transfected at high efficiency and very low cytotoxicity (%50) with plasmid expressing Flag-tagged wtMfn2 or Flag-tag alone by Amaxa rat neuron Nucleofector kit (VGP-1003), according to the manufacturer's instructions. The expression plasmid (p3xFLAG-CMV-10) coding for Flag-tagged wtMfn2 was gently provided by Prof. Nobuhiro Nakamura Department of Biological Sciences, Tokyo Institute of Technology, 4259-B19 Nagatsuta-cho, Midori-ku, Yokohama, 226-8501, Japan.

HeLa cells were transfected using Xfect™ Clontech reagents (Takara Clontech 631318) according to the manufacturer's instructions

Short hairpin RNA (shRNA) interference for Parkin and UCHL-1

Gene silencing of primary hippocampal neurons was carried out by Amaxa rat neuron Nucleofector kit (VGP-1003) according to the manufacturer's instructions. Forty picomoles of shRNA scrambled Parkin or 40 pmol or shRNAParkin (Santa Cruz, sc-270243-SH); 5 μg of shRNA scrambled UCHL1 or 5 μg of shRNA UCHL1 (Origene, TF710038) were used to transfect 5×10^6 cells per sample with the selected program O-003. After 48 h of culturing, the medium was again replaced with fresh culture medium (Neurobasal + 2% B27) and the cells were infected according to (72).

Hexokinase activity

The activity of Hexokinase (HK), which catalyses the reaction ATP + glucose → glucose-6-phosphate (G6P) + ADP, was assayed through a coupled reaction with glucose-6-phosphate dehydrogenase (G6PDH), following the NADP reduction at 340 nm ($\varepsilon_{340\text{-}nm} = 6.22\ mM^{-1}\ cm^{-1}$), using a Jasco double-beam/double-wavelength spectrophotometer UV-550, under V_{max} conditions. The assay was performed at 25°C and pH 7.2 to mimic intracellular pH. The assay mix contained: 5 mM $MgCl_2$, 8 mM ATP, 1 mM NADP, 0.1 U/ml of G6PDH and 0.5 mg cell homogenate. After 10 mM glucose addition to cell homogenate (0.2 mg protein), the activity of HK was determined by following the conversion of NADP to NADPH of the coupled reaction in which G6P is further oxidized to 6-phosphogluconate via G6PDH (158). Enzyme activity was obtained as the tangent to the initial part of the progress curves and expressed, on the basis of protein present in the cell homogenate, as nmol/min (= mU) per mg of protein, where 1 unit of enzyme activity (U) is defined as μmol/min and the specific activity as U/mg protein.

Immunofluorescence

Following treatment, neuronal cultures were washed twice with PBS and fixed in 4% (w/v) paraformaldehyde for 15 min at room temperature. Cells were permeabilized with 0.1% (v/v) Triton X-100/PBS pH 7.4 for 4 min at room temperature. Coverslips were saturated with 2% BSA and 10% normal goat serum (NGS) for 3 h followed by incubation overnight at 4°C in a humidified chamber with primary antibodies. Unbound antibody was removed by three washes and bound antibody was detected by incubation with donkey anti-rabbit Alexa 488 (1:300) and donkey anti-mouse rhodamine-conjugated (1:300) secondary antibodies (Invitrogen) at room temperature for 30 min. Nuclei were stained with nuclear marker 4,6-diamidino-2-phenylindole dihydrochloride (DAPI; Sigma, St Louis, MO, USA) 1:1000 in PBS for 5 min. Controls were performed either by omitting the primary antibody.

Tissue slabs derived from CA1 hippocampal region of AD and ND cases were placed in a solution of 4% paraformaldehyde at +4° for 3 days. After three washes 10 min each, slabs were placed in a solution of 30% (w/v) sucrose in PBS at +4° until they sank. The cryoprotected slabs were cut on a freezing microtome into 40 μm thick sections and collected in a culture well for free floating immunofluorescence procedures. For double immunofluorescence the following primary antibodies were used: anti-Parkin (Park8), mouse 1:100; anti: UCHL-1, mouse 1:100; anti-CCP NH_2 tau rabbit 1:300. After incubation in blocking solution (25% FBS in 0.3% Triton X-100 in TBS) for 2 h at room temperature, sections were incubated with primary antibodies diluted in 20% FBS in 0.3% Triton X-100 in TBS for 48 h at +4°C and, then, for additional 30 min at room temperature. After three washing, sections were incubated with a mix solution of donkey anti-rabbit Alexa 488 (1:100) and donkey anti-mouse rhodamine-conjugated (1:100) secondary antibodies (Invitrogen) diluted in 10% FBS in 0.3% Triton X-100 in TBS for 2 h at room temperature. The sections were next washed three times in TBS and then stained with 0.3% Sudan Black B—to reduce autofluorescence—for 1 min at room temperature, followed by washing in water for three times. Sections were then incubated with the nuclear marker, DNA-fluorochrome 4′,6-diamidino-2-phenylindole (DAPI, 1:1000, Sigma-Aldrich) for 10 min, for nuclei visualization, followed by a further rinse. Sections were mounted on slides, air dried and coverslipped using gel mount (Biomeda Corp., Foster City, CA, USA).

Isolation of mitochondria

Isolation of mitochondria was performed using mitochondrial extraction kit (Qiagen 37 612), as previously described (17). In brief samples were homogenized in 0.5 ml of homogenization buffer using a tissue ruptor rotor-stator and incubated on an end-over-end shaker for 10 min at 4°C. The homogenate was centrifuged at 1000*g* for 10 min at 4°C. The resulting pellet was resuspended in disruption buffer, repeatedly passed through a narrow-gauge needle (26 or 21 gauge) and re-centrifuged at 1000*g* for 10 min; the pellet contains nuclei, cell debris and unbroken cells. The supernatant, which contains mitochondria, was re-centrifuged at 6000*g* for 10 min. The mitochondria pellet was resuspended in mitochondria purification buffer and slowly the disruption buffer was pipetted under the purification buffer. The mitochondrial suspension was pipetted on top of layers and centrifuged at 14 000*g* for 15 min at 4°C. The Mitochondria pellet

was resuspended in mitochondria storage buffer. The purity of mitochondrial preparation was checked by probing fractionated protein extracts with several specific antibodies reacting with mitochondrial markers, as previously described (17).

Isolation of purified synaptosomes and PSD fraction

Purified synaptosomes were prepared as previously described (159,160). Briefly, the tissue was homogenized in 10 volumes of 0.32 M sucrose, buffered to pH 7.4 with Tris-(hydroxymethyl)-amino methane [Tris, final concentration (f.c.) 0.01 M] using a glass/Teflon tissue grinder (clearance 0.25 mm); the homogenate was centrifuged at 1000*g* for 5 min to remove nuclei and debris and the supernatant was gently stratified on a discontinuous Percoll (Sigma-Aldrich, Italy) gradient (2, 6, 10 and 20% v/v in Tris-buffered sucrose) and centrifuged at 33 500*g* for 5 min. The layer between 10 and 20% Percoll (synaptosomal fraction) was collected and washed by centrifugation. The synaptosomal pellets were resuspended in a physiological solution (Standard Medium) with the following composition (mM): NaCl, 140; KCl, 3; $MgSO_4$, 1.2; $CaCl_2$, 1.2; NaH_2PO_4, 1.2; $NaHCO_3$, 5; HEPES, 10; glucose, 10; pH 7.2–7.4. Immediately before fixation procedures, synaptosomes were incubated with MitoTracker red CMxRos (M7512 Molecular Probes, Eugene, OR, USA) at a concentration of 500 for 20 min. After three washing, synaptosomes were seeded for 30 min on coverslip coated with poly-L-lysine (50 μg/ml) at 4°C, washed twice with PBS and fixed in 2% (w/v) freshly prepared paraformaldehyde in PBS for 10 min at room temperature. After four washes synaptosomes were permeabilized with 0.05% (v/v) Triton X-100/PBS for 5 min, washed and incubated overnight in a mix solution of primary antibodies each diluted 1:200 in 0.05% (v/v) Triton X-100/PBS at 4 °C. Following three washes, synaptosomes were incubated with a mix solution of donkey anti-rabbit Alexa 488 (1:500) and donkey anti-mouse Alexa 647 (1:500) secondary antibodies (Invitrogen) for 2 h at 4°C, then coverslip were washed, air dried and mounted on slide using gel mount. Controls were performed by omitting the primary antibodies.

PSD-enriched fraction was prepared according procedure described in (161). Briefly, the brain was rapidly dissected and the hippocampus was homogenized in homogenization buffer (320 mM sucrose, 10 mM Tris–HCl (pH 7.4), 1 mM EDTA, 1 mM $NaHCO_3$, 1 mM PMSF, 1 mM Na_3VO_4, 20 mM β-glycerophosphate, 5 mM NaF, with protease inhibitors; Sigma) with 10 strokes of a tight-fitting glass Dounce tissue grinder (7 ml, Wheaton). The homogenate was centrifuged at 1000*g* for 10 min and the resulting supernatant was centrifuged at 10 000*g* for 15 min. The pellet was resuspended in homogenization buffer with 0.5% Triton X-100 containing protease inhibitors and centrifuged at 32 000*g* for 20 min. The supernatant was referred as extra synaptic membrane enriched fraction while the pellet containing the PSD fraction (Triton X-100 insoluble fraction) was then resuspended in RIPA buffer (50 mM Tris–HCl (pH 7.4), 1% Triton X-100, 0.25% sodium deoxycholate, (wt/vol) 150 mM NaCl, 5 mM $MgCl_2$, 1 mM EDTA, 0.1% SDS (wt/vol), protease inhibitors), sonicated and incubated on ice for 20 min. The samples were centrifuged at 11 500*g* for 10 min and the protein concentration of resulting supernatant was determined.

Protein cellular lysates preparation

Total proteins were extracted by scraping the cells in an SDS-reducing sample buffer or lysis in ice-cold RIPA buffer (50 mM Tris–HCl, pH 8, 150 mM NaCl, 1% Triton, 2 mM EDTA, 0.1% SDS plus proteases inhibitor cocktail (Sigma Aldrich, P8340) and phosphatase inhibitor cocktail (Sigma-Aldrich, P5726/P2850) and centrifuged at 4°C for 15 min at 1000*g*. The supernatant was then collected and boiled for 5 min.

Western blot analysis and densitometry

Equal amounts of protein were subjected to SDS-PAGE 7.5–15% linear gradient or Bis–Tris gel 4–12% (NuPage, Invitrogen). After electroblotting onto a nitrocellulose membrane (Hybond-C Amersham Biosciences, Piscataway, NJ, USA) the filters were blocked in TBS containing 10% non-fat dried milk for 1 h at room temperature or overnight at 4°C. Proteins were visualized using appropriate primary antibodies. All primary antibodies were diluted in TBS and incubated with the nitrocellulose blot overnight at 4°C. Incubation with secondary peroxidase coupled anti-mouse, anti-rabbit or anti-goat antibodies was performed by using the ECL system (Amersham, Arlington Heights, IL, USA) Final figures were assembled by using Adobe Photoshop 6 and Adobe Illustrator 10 and quantitative analysis of acquired images was performed by using ImageJ (http://imagej.nih.gov/ij/).

Confocal microscopy and image analysis

Slides were examined under a confocal laser scanning microscope (Leica SP5, Leica Microsystems, Wetzlar, Germany) equipped with four laser lines: violet diode emitting at 405 nm, argon emitting at 488 nm, helium/neon emitting at 543 nm, helium/neon emitting at 633 nm and a transmitted light detector for differential interference contrast (DIC; Nomarski) imaging. Bright field images were corrected for inhomogeneities of the brightness across the image by using Adobe Photoshop high-pass filter, and edges contrast was enhanced with ImageJ CLAHE (Contrast Limited Adaptive Histogram Equalization; http://rsbweb.nih.gov/ij/plugins/clahe/index.html) filter plugin (block size, 127; histogram bins, 256; maximum slope, 3). Confocal acquisition setting was identical between control and experimental cases. For production of figures, brightness and contrast of images were globally enhanced by using linear histogram correction and slightly over-saturated. The over-saturation enables a better qualitative visual evaluation of both morphological features and colocalization domains. Quantitative image analysis was performed by using Imaris Suite 7.4® (Bitplane A.G., Zurich, Switzerland) or ImageJ 1.4 (imagej.nih.gov/ij/) softwares on five different images derived from each experimental group. Image analysis was performed under visual control to determine thresholds that subtracts background noise and takes into account neuronal structures. During image processing, the images were compared with the original raw data to make sure that no structures were introduced that were not seen in the original data series or that structures present in the original data series were not removed. To determine fluorescent signal colocalization between different channels the ImarisColoc module was used. Before colocalization analysis, a median filter was applied to the images to reduce the background noise and source channels threshold were established by automatic thresholding of the *P*-value. The degree of channels colocalization was analyzed by considering the Pearson's coefficient and thresholded Manders coefficient A and B in colocalized volume. To compare the intensity relations between the fluorescence channels across the morphological features in colocalizion studies the ImageJ tool plot profile was used. To evaluate the fluorescence intensity several masks were drawn on the putative cell bodies, after which the DAPI channel was deleted and measures were performed.

Images of synaptosomes were acquired as described above and deconvolved through a blind deconvolution algorithm by using AutoQuant X3 (Media Cybernetics, Rockville, USA).

Coimmunoprecipitation

The mitochondrial extraction from human purified synaptosomes was performed according to (17) using mitochondrial extraction kit (Qiagen 37612) according to the manufacturer's instructions (see the Isolation of mitochondria section). The synaptic mitochondrial pellet was resuspended in mitochondria storage buffer, the proteins concentration was determined by BCA assay (Dc Protein Assay, BioRad, 500-0116) and then samples were subjected to IP, as previously described (53). In brief, 500 μg mitochondrial proteins extract was lysed using immunoprecipitation (IP) buffer (50 mM Tris, pH 8.0, 150 mM NaCl, 10% glycerol, 0.5 mM EDTA, 0.5 mM EGTA, 50 mM NaF, 1 mM $NaOV_4$, 1% NP40) supplemented with proteases inhibitor cocktail (Sigma-Aldrich, P8340) and phosphatase inhibitor cocktail (Sigma-Aldrich, P5726/P2850). Lysates were then centrifuged at 4°C for 10 min at 1000 *g* and the supernatants were precleared using 10 μl of protein G/A (Invitrogen) for 1 h at 4°C. The pre-cleared protein extracts were immunoprecipitated by magnetic Dynabeads (Invitrogen) according to the manufacturer's instructions using: 4 μg of antiserum CCP NH_2 tau for 20 μl of protein A. The immunocomplexes were eluted with Laemmli buffer 1× plus DTT (Invitrogen) and were next analyzed by immunoblotting with mouse Parkin antibody (Park8clone) and mouse UCHL-1 (clone31A3)

Reciprocal IP was performed on the precleared proteins extracts with rabbit UCHL-1 (EPR4118) 1:10 for 1.5 mg protein extract for 40 μl of protein A. The immunocomplexes were next eluted with Laemmli buffer 1× plus DTT (Invitrogen) and analyzed by immunoblotting with mouse Parkin antibody (Park8clone) and rabbit CCP NH_2 tau antibody.

In several experiments, to eliminate the detection-interference from both heavy-chain (~50 kDa) and light-chain (25 kDa) IgG-fragments, an HRP-conjugated detection secondary antibody, which specifically binds to functional primary antibodies (whole IgG), has been used.

Calpastatin transgenic mice

Transgenic mice expressing human calpastatin (hCAST), under control of the neuron-specific calcium–calmodulin-dependent kinase II α subunit promoter, were gently provided by Prof. Takaomi Saido Riken Brain Science Institute, Saitamo 351-0198, Japan. hCAST mice were created on a C57Bl/6 background and characterized as previously described (95,96) and these mice exhibit a 3-fold increase in calpastatin activity and display no adverse phenotype (96). A colony was established at CNR-EBRI consortium from which hCAST transgenic (Tg) and WT littermates were bred for experimental studies. All mice were housed in controlled conditions under a 14:10 light:dark photoperiod and allowed food and water *ad libitum*. Animal husbandry and surgical procedures were performed in accordance with EEC guidelines (Directive 86/609/CEE). The genotype was determined by PCR with specific primers 5′-CATGAACCACAGACAGCTTGGTTGAC-3′ and 5′-GGAGGATTTGATATTCACCTGGCCCG-3′ that generate a 350-bp product. GADPH forward 5′-ACCACAGTCCATGCCATCAC-3′ and reverse 5′-TCCACCACCCTGTTGCTG-3′ primers were also included as internal control. We finally confirmed that the transgene-derived human calpastatin was robustly expressed in hippocampus and neocortex by western blotting analysis with human-specific calpastatin antibody (clone PI11 Millipore MAB3084), as described in (162).

Statistical analysis

Experiments were carried out in triplicates and repeated at least three times. Data were expressed as means ± SD ($n = 4$). Statistically significant differences were calculated by unpaired two-tailed Student's *t*-test ($^{*}P < 0.05$; $^{**}P < 0.01$; $^{***}P < 0.0001$) as indicted in the figure legends. Data from western blot analysis and immunofluorescence studies were representative of at least three separate experiments.

Supplementary Material

Supplementary Material is available at *HMG* online.

Acknowledgements

We wish to thank Prof. Nobuhiro Nakamura Department of Biological Sciences, Tokyo Institute of Technology, 4259-B19 Nagatsuta-cho, Midori-ku, Yokohama, 226–8501, Japan for providing expression plasmid (p3xFLAG-CMV-10) coding for Flag-tagged wtMfn2. We are also very grateful to Prof. Takaomi Saido Riken Brain Science Institute, Saitamo 351-0198, Japan for providing hCAST mice.

Conflict of Interest statement. None declared.

Funding

This research was supported by grant from FIRB B81J07000070001 and Fondazione Roma to P.C and by grant from PRIN 2010–2011 (prot. 2010M2JARJ-003) to G.A. The funders had no role in study design, data collection and analysis, decision to publish or preparation of manuscript.

References

1. Guillozet-Bongaarts, A.L., Glajch, K.E., Libson, E.G., Cahill, M. E., Bigio, E., Berry, R.W. and Binder, L.I. (2007) Phosphorylation and cleavage of tau in non-AD tauopathies. *Acta Neuropathol.*, **113**, 513–520.
2. García-Sierra, F., Mondragón-Rodríguez, S. and Basurto-Islas, G. (2008) Truncation of tau protein and its pathological significance in Alzheimer's disease. *J. Alzheimers Dis.*, **14**, 401–409.
3. Horowitz, P.M., Patterson, K.R., Guillozet-Bongaarts, A.L., Reynolds, M.R., Carroll, C.A., Weintraub, S.T., Bennett, D.A., Cryns, V.L., Berry, R.W. and Binder, L.I. (2004) Early N-terminal changes and caspase-6 cleavage of tau in Alzheimer's disease. *J. Neurosci.*, **24**, 7895–7902.
4. Wang, Y., Garg, S., Mandelkow, E.M. and Mandelkow, E. (2010) Proteolytic processing of tau. *Biochem. Soc. Trans.*, **38**, 955–961.
5. Reddy, P.H. (2011) Abnormal tau, mitochondrial dysfunction, impaired axonal transport of mitochondria, and synaptic deprivation in Alzheimer's disease. *Brain Res.*, **1415**, 136–148.
6. Manczak, M. and Reddy, P.H. (2012) Abnormal interaction of VDAC1 with amyloid beta and phosphorylated tau causes mitochondrial dysfunction in Alzheimer's disease. *Hum. Mol. Genet.*, **21**, 5131–5146.
7. Du, H., Guo, L., Yan, S., Sosunov, A.A., McKhann, G.M. and Yan, S.S. (2010) Early deficits in synaptic mitochondria in

an Alzheimer's disease mouse model. *Proc. Natl. Acad. Sci. USA*, **107**, 18670–18675.
8. Du, H., Guo, L. and Yan, S.S. (2012) Synaptic mitochondrial pathology in Alzheimer's disease. *Antioxid. Redox. Signal.*, **16**, 1467–1475.
9. Pooler, A.M., Noble, W. and Hanger, D.P. (2014) A role for tau at the synapse in Alzheimer's disease pathogenesis. *Neuropharmacology*, **76**(Pt A), 1–8.
10. Tai, H.C., Serrano-Pozo, A., Hashimoto, T., Frosch, M.P., Spires-Jones, T.L. and Hyman, B.T. (2012) The synaptic accumulation of hyperphosphorylated tau oligomers in Alzheimer disease is associated with dysfunction of the ubiquitin-proteasome system. *Am. J. Pathol.*, **181**, 1426–1435.
11. Upadhya, S.C. and Hegde, A.N. (2007) Role of the ubiquitin proteasome system in Alzheimer's disease. *BMC Biochem.*, **8**(Suppl 1), S12.
12. Hegde, A.N. and DiAntonio, A. (2002) Ubiquitin and the synapse. *Nat. Rev. Neurosci.*, **3**, 854–861.
13. Keck, S., Nitsch, R., Grune, T. and Ullrich, O. (2003) Proteasome inhibition by paired helical filament-tau in brains of patients with Alzheimer's disease. *J. Neurochem.*, **85**, 115–122.
14. Terry, R.D., Masliah, E., Salmon, D.P., Butters, N., DeTeresa, R., Hill, R., Hansen, L.A. and Katzman, R. (1991) Physical basis of cognitive alterations in Alzheimer's disease: synapse loss is the major correlate of cognitive impairment. *Ann. Neurol.*, **30**, 572–580.
15. DeKosky, S.T. and Scheff, S.W. (1990) Synapse loss in frontal cortex biopsies in Alzheimer's disease: correlation with cognitive severity. *Ann. Neurol.*, **27**, 457–464.
16. Rhein, V., Song, X., Wiesner, A., Ittner, L.M., Baysang, G., Meier, F., Ozmen, L., Bluethmann, H., Dröse, S., Brandt, U. *et al.* (2009) Amyloid-beta and tau synergistically impair the oxidative phosphorylation system in triple transgenic Alzheimer's disease mice. *Proc. Natl Acad. Sci. USA*, **106**, 20057–20062.
17. Amadoro, G., Corsetti, V., Atlante, A., Florenzano, F., Capsoni, S., Bussani, R., Mercanti, D. and Calissano, P. (2012) Interaction between NH(2)-tau fragment and Aβ in Alzheimer's disease mitochondria contributes to the synaptic deterioration. *Neurobiol. Aging.*, **33**, 833.e1–833S25.
18. Manczak, M. and Reddy, P.H. (2012) Abnormal interaction between the mitochondrial fission protein Drp1 and hyperphosphorylated tau in Alzheimer's disease neurons: implications for mitochondrial dysfunction and neuronal damage. *Hum. Mol. Genet.*, **21**, 2538–2547.
19. Quintanilla, R.A., Matthews-Roberson, T.A., Dolan, P.J. and Johnson, G.V. (2009) Caspase-cleaved tau expression induces mitochondrial dysfunction in immortalized cortical neurons: implications for the pathogenesis of Alzheimer disease. *J. Biol. Chem.*, **284**, 18754–18766.
20. Quintanilla, R.A., Dolan, P.J., Jin, Y.N. and Johnson, G.V. (2012) Truncated tau and Aβ cooperatively impair mitochondria in primary neurons. *Neurobiol. Aging.*, **33**, 619.e25–35.
21. Eckert, A., Schmitt, K. and Götz, J. (2011) Mitochondrial dysfunction—the beginning of the end in Alzheimer's disease? Separate and synergistic modes of tau and amyloid-β toxicity. *Alzheimers Res. Ther.*, **3**, 15. doi:10.1186/alzrt74.
22. Wang, X., Su, B., Siedlak, S.L., Moreira, P.I., Fujioka, H., Wang, Y., Casadesus, G. and Zhu, X. (2008) Amyloid-β overproduction causes abnormal mitochondrial dynamics via differential modulation of mitochondrial fission/fusion proteins. *Proc. Natl Acad. Sci. USA*, **105**, 19318–19323.
23. Wang, X., Su, B., Lee, H.G., Li, X., Perry, G., Smith, M.A. and Zhu, X. (2009) Impaired balance of mitochondrial fission and fusion in Alzheimer's disease. *J. Neurosci.*, **29**, 9090–9103.
24. Karbowski, M. and Neutzner, A. (2012) Neurodegeneration as a consequence of failed mitochondrial maintenance. *Acta Neuropathol.*, **123**, 157–171.
25. DuBoff, B., Feany, M. and Götz, J. (2013) Why size matters—balancing mitochondrial dynamics in Alzheimer's disease. *Trends Neurosci.*, **36**, 325–335.
26. Zhu, X., Perry, G., Smith, M.A. and Wang, X. (2013) Abnormal mitochondrial dynamics in the pathogenesis of Alzheimer's disease. *J. Alzheimers Dis.*, **33**(Suppl 1), S253–S262.
27. Wang, X., Su, B., Zheng, L., Perry, G., Smith, M.A. and Zhu, X. (2009) The role of abnormal mitochondrial dynamics in the pathogenesis of Alzheimer's disease. *J. Neurochem.*, **109** (Suppl 1), 153–159.
28. Moreira, P.I., Siedlak, S.L., Wang, X., Santos, M.S., Oliveira, C. R., Tabaton, M., Nunomura, A., Szweda, L.I., Aliev, G., Smith, M.A., Zhu, X. and Perry, G. (2007) Increased autophagic degradation of mitochondria in Alzheimer disease. *Autophagy*, **3**, 614–615.
29. Moreira, P.I., Siedlak, S.L., Wang, X., Santos, M.S., Oliveira, C. R., Tabaton, M., Nunomura, A., Szweda, L.I., Aliev, G., Smith, M.A., Zhu, X. and Perry, G. (2007) Autophagocytosis of mitochondria is prominent in Alzheimer disease. *J. Neuropathol. Exp. Neurol.*, **66**, 525–532.
30. Young-Collier, K.J., McArdle, M. and Bennett, J.P. (2012) The dying of the light: mitochondrial failure in Alzheimer's disease. *J. Alzheimers Dis.*, **28**, 771–781.
31. Baloyannis, S.J. (2006) Mitochondrial alterations in Alzheimer's disease. *J. Alzheimers Dis.*, **9**, 119–126.
32. Baloyannis, S.J. (2011) Mitochondria are related to synaptic pathology in Alzheimer's disease. *Int. J. Alzheimers Dis.*, **2011**, 305395.
33. de la Monte, S.M., Luong, T., Neely, T.R., Robinson, D. and Wands, J.R. (2000) Mitochondrial DNA damage as a mechanism of cell loss in Alzheimer's disease. *Lab. Invest.*, **80**, 1323–1335.
34. Xie, H., Guan, J., Borrelli, L.A., Xu, J., Serrano-Pozo, A. and Bacskai, B.J. (2013) Mitochondrial alterations near amyloid plaques in an Alzheimer's disease mouse model. *J. Neurosci.*, **33**, 17042–17051.
35. Bonda, D.J., Wang, X., Perry, G., Smith, M.A. and Zhu, X. (2010) Mitochondrial dynamics in Alzheimer's disease: opportunities for future treatment strategies. *Drugs Aging*, **27**, 181–192.
36. Kamat, P.K., Kalani, A., Kyles, P., Tyagi, S.C. and Tyagi, N. (2014) Autophagy of mitochondria: a promising therapeutic target for neurodegenerative disease. *Cell Biochem Biophys.*, **70**, 707–719.
37. Palikaras, K. and Tavernarakis, N. (2014) Mitochondrial homeostasis: the interplay between mitophagy and mitochondrial biogenesis. *Exp. Gerontol.*, **56**, 182–188.
38. Zhu, J., Wang, K.Z. and Chu, C.T. (2013) After the banquet: mitochondrial biogenesis, mitophagy, and cell survival. *Autophagy*, **9**, 1663–1676.
39. Hung, K.C., Huang, H.J., Lin, M.W., Lei, Y.P. and Lin, A.M. (2014) .Roles of autophagy in MPP+-induced neurotoxicity in vivo: the involvement of mitochondria and α-synuclein aggregation. *PLoS One*, **9**, e91074.
40. Zhu, J.H., Horbinski, C., Guo, F., Watkins, S., Uchiyama, Y. and Chu, C.T. (2000) Regulation of autophagy by extracellular signal-regulated protein kinases during 1-methyl-4-phenyl pyridinium -induced cell death. *Am. J. Pathol.*, **170**, 75–86.

41. Choubey, V., Safiulina, D., Vaarmann, A., Cagalinec, M., Wareski, P., Kuum, M., Zharkovsky, A. and Kaasik, A. (2011) Mutant A53 T alpha-synuclein induces neuronal death by increasing mitochondrial autophagy. *J. Biol. Chem.*, **286**, 10814–10824.
42. Chang, C.F., Huang, H.J., Lee, H.C., Hung, K.C., Wu, R.T. and Lin, A.M. (2012) Melatonin attenuates kainic acid-induced neurotoxicity in mouse hippocampus via inhibition of autophagy and α-synuclein aggregation. *J. Pineal. Res.*, **52**, 312–321.
43. Tzeng, Y.W., Lee, L.Y., Chao, P.L., Lee, H.C., Wu, R.T. and Lin, A.M. (2010) Role of autophagy in protection afforded by hypoxic preconditioning against MPP+-induced neurotoxicity in SH-SY5Y cells. *Free Radic. Biol. Med.*, **49**, 839–846.
44. Escobar-Henriques, M. and Langer, T. (2014) Dynamic survey of mitochondria by ubiquitin. *EMBO Rep.*, **15**, 231–243.
45. Kirkin, V., McEwan, D.G., Novak, I. and Dikic, I. (2009) A role for ubiquitin in selective autophagy. *Mol. Cell*, **34**, 259–269.
46. Amadoro, G., Corsetti, V., Florenzano, F., Atlante, A., Bobba, A., Nicolin, V., Nori, S.L. and Calissano, P. (2014) Morphological and bioenergetic demands underlying the mitophagy in post-mitotic neurons: the pink-parkin pathway. *Front. Aging Neurosci.*, **6**, 18.
47. Reddy, P.H., Tripathi, R., Troung, Q., Tirumala, K., Reddy, T.P., Anekonda, V., Shirendeb, U.P., Calkins, M.J., Reddy, A.P., Mao, P. and Manczak, M. (2012) Abnormal mitochondrial dynamics and synaptic degeneration as early events in Alzheimer's disease: implications to mitochondria-targeted antioxidant therapeutics. *Biochim. Biophys. Acta*, **1822**, 639–649.
48. Grenier, K., McLelland, G.L. and Fon, E.A. (2013) Parkin- and PINK1-dependent mitophagy in neurons: will the real pathway please stand up? *Front. Neurol.*, **4**, 100.
49. Taylor, E.B. and Rutter, J. (2011) Mitochondrial quality control by the ubiquitin-proteasome system. *Biochem. Soc. Trans.*, **39**, 1509–1513.
50. Joselin, A.P., Hewitt, S.J., Callaghan, S.M., Kim, R.H., Chung, Y.H., Mak, T.W., Shen, J., Slack, R.S. and Park, D.S. (2012) ROS-dependent regulation of Parkin and DJ-1 localization during oxidative stress in neurons. *Hum. Mol. Genet.*, **21**, 4888–4903.
51. Koyano, F., Okatsu, K., Ishigaki, S., Fujioka, Y., Kimura, M., Sobue, G., Tanaka, K. and Matsuda, N. (2013) The principal PINK1 and Parkin cellular events triggered in response to dissipation of mitochondrial membrane potential occur in primary neurons. *Genes Cells.*, **18**, 672–681.
52. Cai, Q., Zakaria, H.M., Simone, A. and Sheng, Z.H. (2012) Spatial parkin translocation and degradation of damaged mitochondria via mitophagy in live cortical neurons. *Curr. Biol.*, **22**, 545–552.
53. Cai, Q., Zakaria, H.M. and Sheng, Z.H. (2012) Long time-lapse imaging reveals unique features of PARK2/Parkin-mediated mitophagy in mature cortical neurons. *Autophagy*, **8**, 976–978.
54. Tanaka, A., Cleland, M.M., Xu, S., Narendra, D.P., Suen, D.F., Karbowski, M. and Youle, R.J. (2010) Proteasome and p97 mediate mitophagy and degradation of mitofusins induced by Parkin. *J. Cell Biol.*, **191**, 1367–1380.
55. Chan, N.C., Salazar, A.M., Pham, A.H., Sweredoski, M.J., Kolawa, N.J., Graham, R.L., Hess, S. and Chan, D.C. (2011) Broad activation of the ubiquitin-proteasome system by Parkin is critical for mitophagy. *Hum. Mol. Genet.*, **20**, 1726–1737.
56. Yoshii, S.R., Kishi, C., Ishihara, N. and Mizushima, N. (2011) Parkin mediates proteasome-dependent protein degradation and rupture of the outer mitochondrial membrane. *J. Biol. Chem.*, **286**, 19630–19640.
57. Bingol, B., Tea, J.S., Phu, L., Reichelt, M., Bakalarski, C.E., Song, Q., Foreman, O., Kirkpatrick, D.S. and Sheng, M. (2014) The mitochondrial deubiquitinase USP30 opposes parkin-mediated mitophagy. *Nature*, **510**, 370–375.
58. Osaka, H., Wang, Y.L., Takada, K., Takizawa, S., Setsuie, R., Li, H., Sato, Y., Nishikawa, K., Sun, Y.J., Sakurai, M. *et al.* (2003) Ubiquitin carboxy-terminal hydrolase L1 binds to and stabilizes monoubiquitin in neuron. *Hum. Mol. Genet.*, **12**, 1945–1958.
59. Bizzi, A., Schaetzle, B., Patton, A., Gambetti, P. and Autilio-Gambetti, L. (1991) Axonal transport of two major components of the ubiquitin system: free ubiquitin and ubiquitin carboxyl-terminal hydrolase PGP 9.5. *Brain Res.*, **548**, 292–299.
60. Liu, Y., Fallon, L., Lashuel, H.A., Liu, Z. and Lansbury, P.T. Jr. (2002) The UCH-L1 gene encodes two opposing enzymatic activities that affect alpha-synuclein degradation and Parkinson's disease susceptibility. *Cell*, **111**, 209–218.
61. Cartier, A.E., Djakovic, S.N., Salehi, A., Wilson, S.M., Masliah, E. and Patrick, G.N. (2009) Regulation of synaptic structure by ubiquitin C-terminal hydrolase L1. *J. Neurosci.*, **29**, 7857–7868.
62. Chen, F., Sugiura, Y., Myers, K.G., Liu, Y. and Lin, W. (2010) Ubiquitin carboxyl-terminal hydrolase L1 is required for maintaining the structure and function of the neuromuscular junction. *Proc. Natl Acad. Sci. USA*, **107**, 1636–1641.
63. Gong, B., Cao, Z., Zheng, P., Vitolo, O.V., Liu, S., Staniszewski, A., Moolman, D., Zhang, H., Shelanski, M. and Arancio, O. (2006) Ubiquitin hydrolase Uch-L1 rescues beta-amyloid-induced decreases in synaptic function and contextual memory. *Cell*, **126**, 775–788.
64. Smith, D.L., Pozueta, J., Gong, B., Arancio, O. and Shelanski, M. (2009) Reversal of long-term dendritic spine alterations in Alzheimer disease models. *Proc. Natl Acad. Sci. USA*, **106**, 16877–16882.
65. Guglielmotto, M., Monteleone, D., Boido, M., Piras, A., Giliberto, L., Borghi, R., Vercelli, A., Fornaro, M., Tabaton, M. and Tamagno, E. (2012) Aβ1–42-mediated down-regulation of Uch-L1 is dependent on NF-κB activation and impaired BACE1 lysosomal degradation. *Aging Cell*, **11**, 834–844.
66. Poon, W.W., Carlos, A.J., Aguilar, B.L., Berchtold, N.C., Kawano, C.K., Zograbyan, V., Yaopruke, T., Shelanski, M. and Cotman, C.W. (2013) β-Amyloid (Aβ) oligomers impair brain-derived neurotrophic factor retrograde trafficking by down-regulating ubiquitin C-terminal hydrolase, UCH-L1. *J. Biol. Chem.*, **288**, 16937–16948.
67. Choi, J., Levey, A.I., Weintraub, S.T., Rees, H.D., Gearing, M., Chin, L.S. and Li, L. (2004) Oxidative modifications and down-regulation of ubiquitincarboxyl-terminal hydrolase L1 associated with idiopathic Parkinson'sand Alzheimer's disease. *J. Biol. Chem.*, **279**, 13256–13264.
68. Pasinetti, G.M. (2001) Use of cDNA microarray in the search for molecular markers involved in the onset of Alzheimer's disease dementia. *J. Neurosci. Res.*, **65**, 471–476.
69. Davison, E.J., Pennington, K., Hung, C.C., Peng, J., Rafiq, R., Ostareck-Lederer, A., Ostareck, D.H., Ardley, H.C., Banks, R. E. and Robinson, P.A. (2009) Proteomic analysis of increased Parkin expression and its interactants provides evidence for a role in modulation of mitochondrial function. *Proteomics*, **9**, 4284–4297.
70. Zanon, A., Rakovic, A., Blankenburg, H., Doncheva, N.T., Schwienbacher, C., Serafin, A., Alexa, A., Weichenberger, C. X., Albrecht, M., Klein, C. *et al.* (2013) Profiling of Parkin-

binding partners using tandem affinity purification. *PLoS One*, **8**, e78648.
71. Amadoro, G., Serafino, A.L., Barbato, C., Ciotti, M.T., Sacco, A., Calissano, P. and Canu, N. (2004) Role of N-terminal tau domain integrity on the survival of cerebellar granule neurons. *Cell Death Differ.*, **11**, 217–230.
72. Amadoro, G., Ciotti, M.T., Costanzi, M., Cestari, V., Calissano, P. and Canu, N. (2006) NMDA receptor mediates tau-induced neurotoxicity by calpain and ERK/MAPK activation. *Proc. Natl Acad. Sci. USA*, **103**, 2892–2897.
73. Corsetti, V., Amadoro, G., Gentile, A., Capsoni, S., Ciotti, M.T., Cencioni, M.T., Atlante, A., Canu, N., Rohn, T.T., Cattaneo, A. and Calissano, P. (2008) Identification of a caspase-derived N-terminal tau fragment in cellular and animal Alzheimer's disease models. *Mol. Cell Neurosci.*, **38**, 381–392.
74. Rohn, T.T., Rissman, R.A., Davis, M.C., Kim, Y.E., Cotman, C. W. and Head, E. (2002) Caspase-9 activation and caspase cleavage of tau in the Alzheimer's disease brain. *Neurobiol. Dis.*, **11**, 341–354.
75. Reifert, J., Hartung-Cranston, D. and Feinstein, S.C. (2011) Amyloid beta-mediated cell death of cultured hippocampal neurons reveals extensive Tau fragmentation without increased full-length tau phosphorylation. *J. Biol. Chem.*, **286**, 20797–20811.
76. Park, S.Y. and Ferreira, A. (2005) The generation of a 17 kDa neurotoxic fragment: an alternative mechanism by which tau mediates beta-amyloid-induced neurodegeneration. *J. Neurosci.*, **25**, 5365–5375.
77. Amadoro, G., Corsetti, V., Stringaro, A., Colone, M., D'Aguanno, S., Meli, G., Ciotti, M., Sancesario, G., Cattaneo, A., Bussani, R., Mercanti, D. and Calissano, P. (2010) A NH2 tau fragment targets neuronal mitochondria at AD synapses: possible implications for neurodegeneration. *J. Alzheimers Dis.*, **21**, 445–470.
78. Amadoro, G., Corsetti, V., Sancesario, G.M., Lubrano, A., Melchiorri, G., Bernardini, S., Calissano, P. and Sancesario, G. (2014c) Cerebrospinal fluid levels of a 20–22 kDa NH_2 fragment of human tau provide a novel neuronal injury biomarker in Alzheimer's disease and other dementias. *J. Alzheimers Dis.*, **42**, 211–226.
79. Pristerà, A., Saraulli, D., Farioli-Vecchioli, S., Strimpakos, G., Costanzi, M., di Certo, M.G., Cannas, S., Ciotti, M.T., Tirone, F., Mattei, E., Cestari, V. and Canu, N. (2013) Impact of N-tau on adult hippocampal neurogenesis, anxiety, and memory. *Neurobiol. Aging*, **34**, 2551–2563.
80. Amadoro, G., Corsetti, V., Florenzano, F., Atlante, A., Ciotti, M.T., Mongiardi, M.P., Bussani, R., Nicolin, V., Nori, S.L., Campanella, M. and Calissano, P. (2014) AD-linked, toxic NH2 human tau affects the quality control of mitochondria in neurons. *Neurobiol. Dis.*, **62**, 489–507.
81. Yu, W., Sun, Y., Guo, S. and Lu, B. (2011) The PINK1/Parkin pathway regulates mitochondrial dynamics and function in mammalian hippocampal and dopaminergic neurons. *Hum. Mol. Genet.*, **20**, 3227–3240.
82. Misko, A.L., Sasaki, Y., Tuck, E., Milbrandt, J. and Baloh, R.H. (2012) Mitofusin2 mutations disrupt axonal mitochondrial positioning and promote axon degeneration. *J. Neurosci.*, **32**, 4145–4155.
83. Lee, S., Sterky, F.H., Mourier, A., Terzioglu, M., Cullheim, S., Olson, L. and Larsson, N.G. (2012) Mitofusin 2 is necessary for striatal axonal projections of midbrain dopamine neurons. *Hum. Mol. Genet.*, **21**, 4827–4835.
84. Myeku, N. and Figueiredo-Pereira, M.E. (2011) Dynamics of the degradation of ubiquitinated proteins by proteasomes and autophagy: association with sequestosome 1/p62. *J. Biol. Chem.*, **286**, 22426–22440.
85. Burbulla, L.F., Fitzgerald, J.C., Stegen, K., Westermeier, J., Thost, A.K., Kato, H., Mokranjac, D., Sauerwald, J., Martins, L.M., Woitalla, D. *et al.* (2014) Mitochondrial proteolytic stress induced by loss of mortalin function is rescued by Parkin and PINK1. *Cell Death Dis.*, **5**, e1180.
86. Zhu, J.H., Gusdon, A.M., Cimen, H., Van Houten, B., Koc, E. and Chu, C.T. (2012) Impaired mitochondrial biogenesis contributes to depletion of functional mitochondria in chronic MPP(+) toxicity: dual roles for ERK1/2. *Cell Death Dis.*, **3**, e312.
87. Van Humbeeck, C., Cornelissen, T., Hofkens, H., Mandemakers, W., Gevaert, K., De Strooper, B. and Vandenberghe, W. (2011) Parkin interacts with Ambra1 to induce mitophagy. *J. Neurosci.*, **31**, 10249–10261.
88. Zeiger, S.L., Stankowski, J.N. and McLaughlin, B. (2011) Assessing neuronal bioenergetic status. *Methods Mol. Biol.*, **758**, 215–235.
89. Ziviani, E. and Whitworth, A.J. (2010) How could Parkin-mediated ubiquitination of mitofusin promote mitophagy? *Autophagy*, **6**, 660–662.
90. Jahani-Asl, A., Cheung, E.C., Neuspiel, M., MacLaurin, J.G., Fortin, A., Park, D.S., McBride, H.M. and Slack, R.S. (2007) Mitofusin 2 protects cerebellar granule neurons against injury-induced cell death. *J. Biol Chem.*, **282**, 23788–23798.
91. Misko, A., Jiang, S., Wegorzewska, I., Milbrandt, J. and Baloh, R.H. (2010) Mitofusin 2 is necessary for transport of axonal mitochondria and interacts with the Miro/Milton complex. *J. Neurosci.*, **30**, 4232–4240.
92. Trinchese, F., Fa', M., Liu, S., Zhang, H., Hidalgo, A., Schmidt, S.D., Yamaguchi, H., Yoshii, N., Mathews, P.M., Nixon, R.A. and Arancio, O. (2008) Inhibition of calpains improves memory and synaptic transmission in a mouse model of Alzheimer disease. *J. Clin. Invest.*, **118**, 2796–2807.
93. Rao, M.V., Mohan, P.S., Peterhoff, C.M., Yang, D.S., Schmidt, S.D., Stavrides, P.H., Campbell, J., Chen, Y., Jiang, Y., Paskevich, P.A. *et al.* (2008) Marked calpastatin (CAST) depletion in Alzheimer's disease accelerates cytoskeleton disruption and neurodegeneration: neuroprotection by CAST overexpression. *J. Neurosci.*, **28**, 12241–12254.
94. Jahani-Asl, A., Pilon-Larose, K., Xu, W., MacLaurin, J.G., Park, D.S., McBride, H.M. and Slack, R.S. (2011) The mitochondrial inner membrane GTPase, optic atrophy 1 (Opa1), restores mitochondrial morphology and promotes neuronal survival following excitotoxicity. *J. Biol. Chem.*, **286**, 4772–4782.
95. Takano, J., Tomioka, M., Tsubuki, S., Higuchi, M., Iwata, N., Itohara, S., Maki, M. and Saido, T.C. (2005) Calpain mediates excitotoxic DNA fragmentation via mitochondrial pathways in adult brains: evidence from calpastatin mutant mice. *J. Biol. Chem.*, **280**, 16175–16184.
96. Higuchi, M., Tomioka, M., Takano, J., Shirotani, K., Iwata, N., Masumoto, H., Maki, M., Itohara, S. and Saido, T.C. (2005) Distinct mechanistic roles of calpain and caspase activation in neurodegeneration as revealed in mice overexpressing their specific inhibitors. *J. Biol. Chem.*, **280**, 15229–15237.
97. Rao, M.V., McBrayer, M.K., Campbell, J., Kumar, A., Hashim, A., Sershen, H., Stavrides, P.H., Ohno, M., Hutton, M. and Nixon, R.A. (2014) Specific calpain inhibition by calpastatin prevents tauopathy and neurodegeneration and restores normal lifespan in tau P301L mice. *J. Neurosci.*, **34**, 9222–9234.
98. McCoy, M.K., Kaganovich, A., Rudenko, I.N., Ding, J. and Cookson, M.R. (2014) Hexokinase activity is required for recruitment of parkin to depolarized mitochondria. *Hum. Mol. Genet.*, **23**, 145–156.

99. Wang, X., Winter, D., Ashrafi, G., Schlehe, J., Wong, Y.L., Selkoe, D., Rice, S., Steen, J., LaVoie, M.J. and Schwarz, T.L. (2011) PINK1 and Parkin target Miro for phosphorylation and degradation to arrest mitochondrial motility. *Cell*, **147**, 893–906.
100. Van Laar, V.S. and Berman, S.B. (2013) The interplay of neuronal mitochondrial dynamics and bioenergetics: implications for Parkinson's disease. *Neurobiol. Dis.*, **51**, 43–55.
101. Denison, S.R., Wang, F., Becker, N.A., Schüle, B., Kock, N., Phillips, L.A., Klein, C. and Smith, D.I. (2003) Alterations in the common fragile site gene Parkin in ovarian and other cancers. *Oncogene*, **22**, 8370–8378.
102. Pawlyk, A.C., Giasson, B.I., Sampathu, D.M., Perez, F.A., Lim, K.L., Dawson, V.L., Dawson, T.M., Palmiter, R.D., Trojanowski, J.Q. and Lee, V.M. (2003) Novel monoclonal antibodies demonstrate biochemical variation of brain parkin with age. *J. Biol. Chem.*, **278**, 48120–48128.
103. Chaugule, V.K., Burchell, L., Barber, K.R., Sidhu, A., Leslie, S. J., Shaw, G.S. and Walden, H. (2011) Autoregulation of Parkin activity through its ubiquitin-like domain. *EMBO J.*, **30**, 2853–2867.
104. Zheng, X. and Hunter, T. (2013) Parkin mitochondrial translocation is achieved through a novel catalytic activity coupled mechanism. *Cell Res.*, **23**, 886–897.
105. Koyano, F., Okatsu, K., Kosako, H., Tamura, Y., Go, E., Kimura, M., Kimura, Y., Tsuchiya, H., Yoshihara, H., Hirokawa, T. *et al.* (2014) Ubiquitin is phosphorylated by PINK1 to activate parkin. *Nature*, **510**, 162–166.
106. Meray, R.K. and Lansbury, P.T. Jr. (2007) Reversible monoubiquitination regulates the Parkinson disease-associated ubiquitin hydrolase UCH-L1. *J. Biol. Chem.*, **282**, 10567–10575.
107. Rakovic, A., Shurkewitsch, K., Seibler, P., Grünewald, A., Zanon, A., Hagenah, J., Krainc, D. and Klein, C. (2013) PTEN-induced putative kinase 1 (PINK1)-dependent ubiquitination of endogenous Parkin attenuates mitophagy: study in human primary fibroblasts and induced pluripotent stem (iPS) cell-derived neurons. *J. Biol. Chem.*, **288**, 2223–2237.
108. Cartier, A.E., Ubhi, K., Spencer, B., Vazquez-Roque, R.A., Kosberg, K.A., Fourgeaud, L., Kanayson, P., Patrick, C., Rockenstein, E., Patrick, G.N. and Masliah, E. (2012) Differential effects of UCHL1 modulation on alpha-synuclein in PD-like models of alpha-synucleinopathy. *PLoS One*, **7**, e34713.
109. Kabuta, T. and Wada, K. (2008) Insights into links between familial and sporadic Parkinson's disease: physical relationship between UCH-L1 variants and chaperone-mediated autophagy. *Autophagy*, **4**, 827–829.
110. Kabuta, T., Furuta, A., Aoki, S., Furuta, K. and Wada, K. (2008) Aberrant interaction between Parkinson disease-associated mutant UCH-L1 and the lysosomal receptor for chaperone-mediated autophagy. *J. Biol. Chem.*, **283**, 23731–23738.
111. Liu, Z., Meray, R.K., Grammatopoulos, T.N., Fredenburg, R.A., Cookson, M.R., Liu, Y., Logan, T. and Lansbury, P.T. Jr. (2009) Membrane-associated farnesylated UCH-L1 promotes alpha-synuclein neurotoxicity and is a therapeutic target for Parkinson's disease. *Proc. Natl Acad. Sci. USA*, **106**, 4635–4640.
112. Cuadrado-Tejedor, M., Cabodevilla, J.F., Zamarbide, M., Gómez-Isla, T., Franco, R. and Perez-Mediavilla, A. (2013) Age-related mitochondrial alterations without neuronal loss in the hippocampus of a transgenic model of Alzheimer's disease. *Curr. Alzheimer Res.*, **10**, 390–405.
113. Calkins, M.J., Manczak, M., Mao, P., Shirendeb, U. and Reddy, P.H. (2011) Impaired mitochondrial biogenesis, defective axonal transport of mitochondria, abnormal mitochondrial dynamics and synaptic degeneration in a mouse model of Alzheimer's disease. *Hum. Mol. Genet.*, **20**, 4515–4529.
114. Varghese, M., Zhao, W., Wang, J., Cheng, A., Qian, X., Chaudhry, A., Ho, L. and Pasinetti, G.M. (2011) Mitochondrial bioenergetics is defective in presymptomatic Tg2576 AD mice. *Transl Neurosci.*, **2**, doi:10.2478/s13380-011-0011-8.
115. Trushina, E., Nemutlu, E., Zhang, S., Christensen, T., Camp, J., Mesa, J., Siddiqui, A., Tamura, Y., Sesaki, H., Wengenack, T. M., Dzeja, P.P. and Poduslo, J.F. (2012) Defects in mitochondrial dynamics and metabolomic signatures of evolving energetic stress in mouse models of familial Alzheimer's disease. *PLoS One*, **7**, e32737.
116. Bai, F. and Witzmann, F. (2007) Synaptosome proteomics. *Subcell Biochem.*, **43**, 77–98.
117. Gillardon, F., Rist, W., Kussmaul, L., Vogel, J., Berg, M., Danzer, K., Kraut, N. and Hengerer, B. (2007) Proteomic and functional alterations in brain mitochondria from Tg2576 mice occur before amyloid plaque deposition. *Proteomics*, **7**, 605–616.
118. Harris, J.A., Koyama, A., Maeda, S., Ho, K., Devidze, N., Dubal, D.B., Yu, G.Q., Masliah, E. and Mucke, L. (2012) Human P301L-mutant tau expression in mouse entorhinal-hippocampal network causes tau aggregation and presynaptic pathology but no cognitive deficits. *PLoS One*, **7**, e45881.
119. Polydoro, M., Dzhala, V.I., Pooler, A.M., Nicholls, S.B., McKinney, A.P., Sanchez, L., Pitstick, R., Carlson, G.A., Staley, K.J., Spires-Jones, T.L. and Hyman, B.T. (2014) Soluble pathological tau in the entorhinal cortex leads to presynaptic deficits in an early Alzheimer's disease model. *Acta Neuropathol.*, **127**, 257–270.
120. Mohamed, N.V., Herrou, T., Plouffe, V., Piperno, N. and Leclerc, N. (2013) Spreading of tau pathology in Alzheimer's disease by cell-to-cell transmission. *Eur. J .Neurosci.*, **37**, 1939–1948.
121. Cherra, S.J. III and Chu, C.T. (2008) Autophagy in neuroprotection and neurodegeneration: a question of balance. *Future Neurol.*, **3**, 309–323.
122. Cherra, S.J. III, Steer, E., Gusdon, A.M., Kiselyov, K. and Chu, C.T. (2013) Mutant LRRK2 elicits calcium imbalance and depletion of dendritic mitochondria in neurons. *Am. J. Pathol.*, **182**, 474–484.
123. Wong, A.S., Lee, R.H., Cheung, A.Y., Yeung, P.K., Chung, S.K., Cheung, Z.H. and Ip, N.Y. (2011) Cdk5-mediated phosphorylation of endophilin B1 is required for induced autophagy in models of Parkinson's disease. *Nat Cell Biol.*, **13**, 568–579. Erratum in Nat Cell Biol., 2011;13:734.
124. Zhu, J.H., Horbinski, C., Guo, F., Watkins, S., Uchiyama, Y. and Chu, C.T. (2007) Regulation of autophagy by extracellular signal-regulated protein kinases during 1-methyl-4-phenylpyridinium-induced cell death. *Am. J. Pathol.*, **170**, 75–86.
125. Inoue, K., Rispoli, J., Kaphzan, H., Klann, E., Chen, E.I., Kim, J., Komatsu, M. and Abeliovich, A. (2012) Macroautophagy deficiency mediates age-dependent neurodegeneration through a phospho-tau pathway. *Mol. Neurodegener.*, **7**, 48.
126. Pacheco, C.D., Elrick, M.J. and Lieberman, A.P. (2009) Tau deletion exacerbates the phenotype of Niemann-Pick type C mice and implicates autophagy in pathogenesis. *Hum. Mol. Genet.*, **18**, 956–965.
127. Chinta, S.J., Mallajosyula, J.K., Rane, A. and Andersen, J.K. (2010) Mitochondrial α-synuclein accumulation impairs complex I function in dopaminergic neurons and results in increased mitophagy in vivo. *Neurosci. Lett.*, **486**, 235–239.
128. Fournier, M., Vitte, J., Garrigue, J., Langui, D., Dullin, J.P., Saurini, F., Hanoun, N., Perez-Diaz, F., Cornilleau, F., Joubert,

C. *et al.* (2009) Parkin deficiency delays motor decline and disease manifestation in a mouse model of synucleinopathy. *PLoS One*, **4**, e6629.
129. Fournier, M., Roux, A., Garrigue, J., Muriel, M.P., Blanche, P., Lashuel, H.A., Anderson, J.P., Barbour, R., Huang, J., du Montcel, S.T., Brice, A. and Corti, O. (2013) Parkin depletion delays motor decline dose-dependently without overtly affecting neuropathology in α-synuclein transgenic mice. *BMC Neurosci.*, **14**, 135. doi:10.1186/1471-2202-14-135.
130. Solano, R.M., Casarejos, M.J., Gómez, A., Perucho, J., de Yébenes, J.G. and Mena, M.A. (2012) Parkin Null Cortical Neuronal/glial cultures are resistant to amyloid-β1-42 toxicity: a role for autophagy? *J. Alzheimers Dis.*, **32**, 57–76.
131. Campello, S., Strappazzon, F. and Cecconi, F. (2014) Mitochondrial dismissal in mammals, from protein degradation to mitophagy. *Biochim. Biophys. Acta*, **1837**, 451–460.
132. Harada, T., Harada, C., Wang, Y.L., Osaka, H., Amanai, K., Tanaka, K., Takizawa, S., Setsuie, R., Sakurai, M., Sato, Y., Noda, M. and Wada, K. (2004) Role of ubiquitin carboxy terminal hydrolase-L1 in neural cell apoptosis induced by ischemic retinal injury in vivo. *Am. J. Pathol.*, **164**, 59–64.
133. Yasuda, T., Nihira, T., Ren, Y.R., Cao, X.Q., Wada, K., Setsuie, R., Kabuta, T., Wada, K., Hattori, N., Mizuno, Y. and Mochizuki, H. (2009) Effects of UCH-L1 on alpha-synuclein overexpression mouse model of Parkinson's disease. *J. Neurochem.*, **108**, 932–944.
134. Wei, K., Wang, P. and Miao, C.Y. (2012) A double-edged sword with therapeutic potential: an updated role of autophagy in ischemic cerebral injury. *CNS Neurosci. Therap.*, **18**, 879–886.
135. Walters, B.J., Campbell, S.L., Chen, P.C., Taylor, A.P., Schroeder, D.G., Dobrunz, L.E., Artavanis-Tsakonas, K., Ploegh, H.L., Wilson, J.A., Cox, G.A. and Wilson, S.M. (2008) Differential effects of Usp14 and Uch-L1 on the ubiquitin proteasome system and synaptic activity. *Mol. Cell Neurosci.*, **39**, 539–548.
136. Kyratzi, E., Pavlaki, M. and Stefanis, L. (2008) The S18Y polymorphic variant of UCH-L1 confers an antioxidant function to neuronal cells. *Hum. Mol. Genet.*, **17**, 2160–2171.
137. Di Domenico, F., Coccia, R., Cocciolo, A., Murphy, M.P., Cenini, G., Head, E., Butterfield, D.A., Giorgi, A., Schinina, M.E., Mancuso, C., Cini, C. and Perluigi, M. (2013) Impairment of proteostasis network in Down syndrome prior to the development of Alzheimer's disease neuropathology: redox proteomics analysis of human brain. *Biochim. Biophys. Acta*, **1832**, 1249–1259.
138. Butterfield, D.A., Gnjec, A., Poon, H.F., Castegna, A., Pierce, W.M., Klein, J.B. and Martins, R.N. (2006) Redox proteomics identification of oxidatively modified brain proteins in inherited Alzheimer's disease: an initial assessment. *J. Alzheimers Dis.*, **10**, 391–397.
139. Sultana, R., Boyd-Kimball, D., Cai, J., Pierce, W.M., Klein, J.B., Merchant, M. and Butterfield, D.A. (2007) Proteomics analysis of the Alzheimer's disease hippocampal proteome. *J. Alzheimers Dis.*, **11**, 153–164.
140. Castegna, A., Aksenov, M., Aksenova, M., Thongboonkerd, V., Klein, J.B., Pierce, W.M., Booze, R., Markesbery, W.R. and Butterfield, D.A. (2002) Proteomic identification of oxidatively modified proteins in Alzheimer's disease brain. Part I: creatine kinase BB, glutamine synthase, and ubiquitin carboxy-terminal hydrolase L-1. *Free Radic. Biol. Med.*, **33**, 562–571.
141. Donovan, L.E., Higginbotham, L., Dammer, E.B., Gearing, M., Rees, H.D., Xia, Q., Duong, D.M., Seyfried, N.T., Lah, J.J. and Levey, A.I. (2012) Analysis of a membrane-enriched proteome from postmortem human brain tissue in Alzheimer's disease. *Proteomics Clin. Appl.*, **6**, 201–211.
142. Cottrell, B.A., Galvan, V., Banwait, S., Gorostiza, O., Lombardo, C.R., Williams, T., Schilling, B., Peel, A., Gibson, B., Koo, E. H., Link, C.D. and Bredesen, D.E. (2005) A pilot proteomic study of amyloid precursor interactors in Alzheimer's disease. *Ann. Neurol.*, **58**, 277–289.
143. Xue, S. and Jia, J. (2006) Genetic association between Ubiquitin Carboxy-terminal Hydrolase-L1 gene S18Y polymorphism and sporadic Alzheimer's disease in a Chinese Han population. *Brain Res.*, **1087**, 28–32.
144. Kumar, P., Pradhan, K., Karunya, R., Ambasta, R.K. and Querfurth, H.W. (2012) Cross-functional E3 ligases Parkin and C-terminus Hsp70-interacting protein in neurodegenerative disorders. *J. Neurochem.*, **120**, 350–370.
145. Burns, M.P., Zhang, L., Rebeck, G.W., Querfurth, H.W. and Moussa, C.E. (2009) Parkin promotes intracellular Abeta1-42 clearance. *Hum. Mol. Genet.*, **18**, 3206–3216.
146. Rodríguez-Navarro, J.A., Gómez, A., Rodal, I., Perucho, J., Martinez, A., Furió, V., Ampuero, I., Casarejos, M.J., Solano, R.M., de Yébenes, J.G. and Mena, M.A. (2008) Parkin deletion causes cerebral and systemic amyloidosis in human mutated tau over-expressing mice. *Hum. Mol. Genet.*, **17**, 3128–3143.
147. Chung, K.K., Thomas, B., Li, X., Pletnikova, O., Troncoso, J.C., Marsh, L., Dawson, V.L. and Dawson, T.M. (2004) S-nitrosylation of parkin regulates ubiquitination and compromises parkin's protective function. *Science*, **304**, 1328–1331.
148. Ko, H.S., Lee, Y., Shin, J.H., Karuppagounder, S.S., Gadad, B.S., Koleske, A.J., Pletnikova, O., Troncoso, J.C., Dawson, V.L. and Dawson, T.M. (2010) Phosphorylation by the c-Abl protein tyrosine kinase inhibits parkin's ubiquitination and protective function. *Proc. Natl Acad. Sci. USA*, **107**, 16691–16696.
149. LaVoie, M.J., Ostaszewski, B.L., Weihofen, A., Schlossmacher, M.G. and Selkoe, D.J. (2005) Dopamine covalently modifies and functionally inactivates parkin. *Nat. Med.*, **11**, 1214–1221.
150. Wang, C., Ko, H.S., Thomas, B., Tsang, F., Chew, K.C., Tay, S. P., Ho, M.W., Lim, T.M., Soong, T.W., Pletnikova, O. *et al.* (2005) Stress-induced alterations in parkin solubility promote parkin aggregation and compromise parkin's protective function. *Hum. Mol. Genet.*, **14**, 3885–3897.
151. Lonskaya, I., Shekoyan, A.R., Hebron, M.L., Desforges, N., Algarzae, N.K. and Moussa, C.E. (2013) Diminished parkin solubility and co-localization with intraneuronal amyloid-β are associated with autophagic defects in Alzheimer's disease. *J. Alzheimers Dis.*, **33**, 231–247.
152. Kalia, S.K., Lee, S., Smith, P.D., Liu, L., Crocker, S.J., Thorarinsdottir, T.E., Glover, J.R., Fon, E.A., Park, D.S. and Lozano, A.M. (2004) BAG5 inhibits parkin and enhances dopaminergic neuron degeneration. *Neuron*, **44**, 931–945.
153. Avraham, E., Rott, R., Liani, E., Szargel, R. and Engelender, S. (2007) Phosphorylation of Parkin by the cyclin-dependent kinase 5 at the linker region modulates its ubiquitin-ligase activity and aggregation. *J. Biol. Chem.*, **282**, 12842–12850.
154. Choo, Y.S., Vogler, G., Wang, D., Kalvakuri, S., Iliuk, A., Tao, W.A., Bodmer, R. and Zhang, Z. (2012) Regulation of parkin and PINK1 by neddylation. *Hum. Mol. Genet.*, **21**, 2514–2523.
155. Soto, A.M. and Sonnenschein, C. (1985) The role of estrogen on the proliferation of human breast tumor cells (MCF-7). *J. Steroid. Biochem.*, **23**, 87–94.
156. Volontè, C., Ciotti, M.T. and Battistini, L. (1994) Development of a method for measuring cell number: application to CNS primary neuronal culture. *Cytometry*, **17**, 274–276.

157. Manthorpe, M., Fagnani, R., Skaper, S.D. and Varon, S. (1986) An automated colorimetric microassay for neuronotrophic factors. *Brain Res.*, **390**, 191–198.
158. Santiago, A.P., Chaves, E.A., Oliveira, M.F. and Galina, A. (2008) Reactive oxygen species generation is modulated by mitochondrial kinases: correlation with mitochondrial antioxidant peroxidases in rat tissues. *Biochimie*, **90**, 1566–1577.
159. Pittaluga, A., Segantini, D., Feligioni, M. and Raiteri, M. (2005) Extracellular protons differentially potentiate the responses of native AMPA receptor subtypes regulating neurotransmitter release. *Br. J. Pharmacol.*, **144**, 293–299.
160. Pittaluga, A., Feligioni, M., Longordo, F., Luccini, E. and Raiteri, M. (2006) Trafficking of presynaptic AMPA receptors mediating neurotransmitter release: neuronal selectivity and relationships with sensitivity to cyclothiazide. *Neuropharmacology*, **50**, 286–296.
161. Davies, K.D., Alvestad, R.M., Coultrap, S.J. and Browning, M. D. (2007) αCAMKII autophosphorylation levels differ depending on subcellular localization. *Brain Res.*, **1158**, 39–49.
162. Schoch, K.M., Evans, H.N., Brelsfoard, J.M., Madathil, S.K., Takano, J., Saido, T.C. and Saatman, K.E. (2012) Calpastatin overexpression limits calpain-mediated proteolysis and behavioral deficits following traumatic brain injury. *Exp. Neurol.*, **236**, 371–282.